4.02 Seismic Source Theory

R Madariaga, Laboratoire de Géologie Ecole Normale Supérieure, Paris, France

4.02.1 Introduction

Earthquake source dynamics provides key elements for the prediction of ground motion and to understand the physics of earthquake initiation, propagation, and healing. The simplest possible model of seismic source is that of a point source buried in an elastic half-space. The development of a proper model of the seismic source took more than 50 years since the first efforts by Nakano (1923) and colleagues in Japan. Earthquakes were initially modeled as simple explosions, then as the result of the displacement of conical surfaces, and finally as the result of fast transformational strains inside a sphere. In the early 1950s, it was recognized that P-waves radiated by earthquakes presented a spatial distribution similar to that produced by single couples of forces, but it was very soon recognized that this type of source could not explain S-wave radiation (Honda, 1962). The next level of complexity was to introduce a double-couple source, a source without resultant force nor moment. The physical origin of the double-couple model was established in the early 1960s thanks to the observational work of numerous seismologists and the crucial theoretical breakthrough of Maruyama (1963) and Burridge and Knopoff (1964) who proved that a fault in an elastic model was equivalent to a double-couple source.

In this chapter, we shall review what we believe are the essential results obtained in the field of kinematic earthquake rupture to date. In **Section 4.02.2**, we review the classical point source model of elastic wave radiation and establish some basic general properties of energy radiation by that source. In **Section 4.02.3**, we discuss the now classical seismic moment tensor source. In **Section 4.02.4**, we discuss extended kinematic sources including the simple rectangular fault model proposed by Haskell (1964, 1966) and a circular model that tries to capture some essential features of crack models. **Section 4.02.5** introduces crack models without friction as models of shear faulting in the earth. This will help establish some basic results that are useful in the study of dynamic models of the earthquake source.

 http://dx.doi.org/10.1016/B978-0-444-53802-4.00070-1

4.02.2 Seismic Wave Radiation from a Point Force: The Green Function

There are many ways of solving the elastic wave equation for different types of initial conditions, boundary conditions, sources, etc. Each of these methods requires a specific approach for every different problem that we would need to study. Ideally, we would like, however, to find a general solution method that would allow us to solve any problem by a simple method. The basic building block of such a general solution method is the Green function, the solution of the following elementary problem: find the radiation from a point source in a finite heterogeneous elastic medium. For simplicity, we consider first the particular case of a homogeneous elastic isotropic medium, for which we know how to calculate the Green function. This will let us establish a general framework for studying more elaborate source models.

4.02.2.1 Seismic Radiation from a Point Source

The simplest possible source of elastic waves is a point force of arbitrary orientation located inside an infinite homogeneous, isotropic elastic body of density ρ, and elastic constants λ and μ. Let $\alpha=\sqrt{(\lambda+2\mu)/\rho}$ and $\beta=\sqrt{\mu/\rho}$ be the P- and S-wave speeds, respectively. Let us note $\mathbf{u}(\mathbf{x},t)$, the particle displacement vector. We have to find the solution of the elastodynamic wave equation:

$$\rho\frac{\partial^2}{\partial t^2}\mathbf{u}(\mathbf{x},t)=(\lambda+\mu)\nabla(\nabla\cdot\mathbf{u}(\mathbf{x},t))+\mu\nabla^2\mathbf{u}(\mathbf{x},t)+\mathbf{f}(\mathbf{x},t) \quad [1]$$

under homogeneous initial conditions, that is, $\mathbf{u}(\mathbf{x},0)=\dot{\mathbf{u}}(\mathbf{x},0)=0$, and the appropriate radiation conditions at infinity. In [1], $\mathbf{f}$ is a general distribution of force density as a function of position and time. For a point force of arbitrary orientation located at a point $\mathbf{x}_0$, the body force distribution is

$$\mathbf{f}(\mathbf{x},t)=\mathbf{f}s(t)\delta(\mathbf{x}-\mathbf{x}_0) \quad [2]$$

where $s(t)$ is the source time function, the variation of the amplitude of the force as a function of time. And $\mathbf{f}$ is a unit vector in the direction of the unit force.

The solution of eqn [1] is easier to obtain in the Fourier transformed domain. As is usual in seismology, we use the following definition of the Fourier transform and its inverse:

$$\begin{aligned}\widetilde{u}(x,\omega)&=\int_{-\infty}^{\infty}u(x,t)\mathrm{e}^{-i\omega t}\mathrm{d}t\\ u(x,t)&=\frac{1}{2\pi}\int_{-\infty}^{\infty}\widetilde{u}(x,\omega)\mathrm{e}^{-i\omega t}\mathrm{d}\omega\end{aligned} \quad [3]$$

Here and in the following, we will note Fourier transform with a tilde.

After some lengthy work see, for example, Achenbach (1975), we find the Green function in the Fourier domain:

$$\begin{aligned}\widetilde{\mathbf{u}}(R,\omega)=&\frac{1}{4\pi\rho}\left[\mathbf{f}\cdot\nabla\nabla\left(\frac{1}{R}\right)\right]\frac{\widetilde{s}(\omega)}{\omega^2}\left[-\left(1+\frac{i\omega R}{\alpha}\right)\mathrm{e}^{-i\omega R/\alpha}\right.\\&\left.+\left(1+\frac{i\omega R}{\beta}\right)\mathrm{e}^{-i\omega R/\beta}\right]\\&+\frac{1}{4\pi\rho\alpha^2}\frac{1}{R}(\mathbf{f}\cdot\nabla R)\nabla R\widetilde{s}(\omega)\mathrm{e}^{-i\omega R/\alpha}\\&+\frac{1}{4\pi\rho\beta^2}\frac{1}{R}[\mathbf{f}-(\mathbf{f}\cdot\nabla R)\nabla R]\widetilde{s}(\omega)\mathrm{e}^{-i\omega R/\beta}\end{aligned} \quad [4]$$

where $R=\|\mathbf{x}-\mathbf{x}_0\|$ is the distance from the source to the observation point. Using the inverse Fourier transform, we can transform eqn [4] to the time domain to obtain the final result

$$\begin{aligned}\mathbf{u}(R,t)=&\frac{1}{4\pi\rho}[\mathbf{f}\cdot\nabla\nabla(1R)]\int_{R/\alpha}^{\min(t,R/\beta)}\tau s(t-\tau)\mathrm{d}\tau\\&+\frac{1}{4\pi\rho\alpha^2}\frac{1}{R}[(\mathbf{f}\cdot\nabla R)\nabla R]s(t-R/\alpha)\\&+\frac{1}{4\pi\rho\beta^2}\frac{1}{R}[\mathbf{f}-(\mathbf{f}\cdot\nabla R)\nabla R]s(t-R/\beta)\end{aligned} \quad [5]$$

This complicated-looking expression can be better understood considering each of its terms separately. The first line is the near field, which comprises all the terms that decrease at long distance from the source faster than R^{-1}. The last two lines are the far-field P and S spherical waves that decrease with distance like R^{-1}.

4.02.2.2 Far-Field Body Waves Radiated by a Point Force

Much of the practical work of seismology is done in the far field, at distances of several wavelengths from the source. When the distance R is large, only the last two terms in [5] are important. Under what conditions can we neglect the first term of that expression with respect to the last two? For that purpose, we notice that in [4], R appears always in the particular combination $\omega R/\alpha$ or $\omega R/\beta$. Clearly, these two ratios determine the far-field conditions. Since $\alpha>\beta$, we conclude that the far field is defined by

$$\frac{\omega R}{\alpha}\gg 1 \quad \text{or} \quad \frac{R}{\lambda}\ll 1$$

where $\lambda=2\pi\alpha/\omega$ is the wavelength of a P-wave of circular frequency ω. The condition for the far field depends therefore on the characteristic frequency or wavelength of the radiation. Thus, depending on the frequency content of the signal $\widetilde{S}(\omega)$, we will be in the far field for high-frequency waves, but we may be in the near field for the low-frequency components.

The far-field radiation from a point force is usually written in the following, shorter form:

$$\begin{aligned}\mathbf{u}^{\mathrm{P}}_{\mathrm{FF}}(R,t)&=\frac{1}{4\pi\rho\alpha^2}\frac{1}{R}\mathfrak{R}^{\mathrm{P}}s(t-R/\alpha)\\ \mathbf{u}^{\mathrm{S}}_{\mathrm{FF}}(R,t)&=\frac{1}{4\pi\rho\beta^2}\frac{1}{R}\mathfrak{R}^{\mathrm{S}}s(t-R/\beta)\end{aligned} \quad [6]$$

where $\mathfrak{R}^{\mathrm{P}}$ and $\mathfrak{R}^{\mathrm{S}}$ are the radiation patterns of P- and S-waves, respectively. Noting that $\nabla R=\mathbf{e}_R$, the unit vector in the radial direction, we can write the radiation patterns in the following simplified form: $\mathfrak{R}^{\mathrm{P}}=f_R\mathbf{e}_R$ and $\mathfrak{R}^{\mathrm{S}}=\mathbf{f}_{\mathrm{T}}=\mathbf{f}-f_{\mathrm{R}}\mathbf{e}_{\mathrm{R}}$ where f_{R} is the radial component of the point force $\mathbf{f}$ and $\mathbf{f}_{\mathrm{T}}$ its transverse component.

Thus, in the far field of a point force, P-waves propagate the radial component of the point force, while the S-waves propagate information about the transverse component of the S-wave. Expressing the amplitude of the radial and transverse component of $\mathbf{f}$ in terms of the azimuth θ of the ray with respect to the applied force, we can rewrite the radiation patterns in the simpler form

$$\Re^{\mathrm{P}} = \cos\theta \mathbf{e}_{\mathrm{R}}, \quad \Re^{\mathrm{S}} = \sin\theta \mathbf{e}_{\Gamma} \qquad [7]$$

As we could expect from the natural symmetry of the problem, the radiation patterns are axially symmetrical about the axis of the point force. P-waves from a point force have a typical dipolar radiation pattern, while S-waves have a toroidal (doughnut-shaped) distribution of amplitudes.

4.02.2.3 The Near Field of a Point Force

When $\omega R/\alpha$ is not large compared to one, all the terms in eqns [4] and [5] are of equal importance. In fact, both far- and near-field terms are of the same order of magnitude near the point source. In order to find the small R behavior, it is preferable to go back to the frequency domain expression [4]. When $R \to 0$, the term in brackets in the first line tends to zero. In order to calculate the near-field behavior, we have to expand the exponentials to order R^2. After some algebra, we find

$$\mathbf{u}(R,t) = \frac{1}{8\pi\rho\beta^2}\frac{1}{R}\left[(\mathbf{f}\cdot\nabla R)\nabla R\left(1-\beta^2/\alpha^2\right) + \mathbf{f}\left(1+\beta^2/\alpha^2\right)\right]s(t) \qquad [8]$$

This is the product of the source time function $s(t)$ with the static displacement produced by a point force of orientation $\mathbf{f}$. This is one of the most important results of static elasticity and is frequently referred to as the Kelvin or Somigliana solution (Aki and Richards, 2002).

The result [8] is quite interesting and somewhat unexpected. The radiation from a point source decays like R^{-1} in the near field, exactly like the far-field terms. This result has been remarked and extensively used in the formulation of regularized boundary integral equations for elastodynamics (Fukuyama and Madariaga, 1995; Hirose and Achenbach, 1989).

4.02.2.4 Energy Flow from Point Force Sources

A very important issue in seismology is the amount of energy radiated by seismic sources. The flow of energy across any surface that encloses the point source must be the same, so that seismic energy is defined for any arbitrary surface. Let us take the scalar product of eqn [1] with the particle velocity $\dot{\mathbf{u}}$ and integrate on a volume V enclosing the single point source located at $\mathbf{x}_0$:

$$\int_V \rho\dot{\mathbf{u}}_i\ddot{\mathbf{u}}_i \mathrm{d}V = \int_V \sigma_{ij,j}\dot{u}_i \mathrm{d}V \int_V f_i\dot{u}_i \mathrm{d}V \qquad [9]$$

where we use dots to indicate time derivatives and the summation convention on repeated indices. In [9], we have rewritten the right-hand side of [1] in terms of the stresses $\sigma_{ij} = \lambda\varepsilon_{ii}\delta_{ij} + 2\mu\varepsilon_{ij}$, where the strains are $\varepsilon_{ij} = 1/2(\partial_j u_i + \partial_j u_i)$.

Using $\sigma_{ij,j}\dot{u}_i = \left(\sigma_{ij}\dot{u}_i\right)_{,j} - \sigma_{ij}\dot{\varepsilon}_{ij}$ and Gauss' theorem, we get the energy flow identity

$$\frac{\mathrm{d}}{\mathrm{d}t}(K(t)+U(t)) = \int_S \sigma_{ij}\dot{u}_i n_j \mathrm{d}S + \int_U f_i\dot{u}_i \mathrm{d}V \qquad [10]$$

where $\mathbf{n}$ is the outward normal to the surface S (see Figure 1). In [10], K is the kinetic energy contained in volume V at time t:

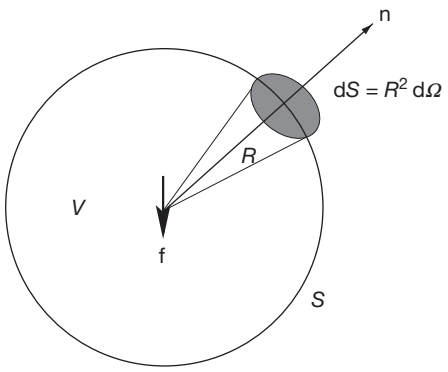

Figure 1 Geometry for computing radiated energy from a point source. The source is at the origin and the observer at a position defined by the spherical coordinates R, θ, ϕ, distance, polar angle, and azimuth.

$$K(t) = \frac{1}{2}\int_V \rho\dot{\mathbf{u}}^2 \mathrm{d}V \qquad [11]$$

while

$$U(t) = \frac{1}{2}\int_V \left[\lambda(\nabla\cdot\mathbf{u})^2 + 2\mu\varepsilon_{ij}\varepsilon_{ij}\right]\mathrm{d}V \qquad [12]$$

is the strain energy change inside the same volume. The last term in [10] is the rate of work of the force against elastic displacement. Equation [10] is the basic energy conservation statement for elastic sources. It says that the rate of energy change inside the body V is equal to the rate of work of the sources $\mathbf{f}$ plus the inward energy flow across the boundary S. This energy balance equation can be extended to study energy flow for moment tensor sources and for cracks (Kostrov and Das, 1988).

Let us note that in [10], energy flows into the body through the surface S. In seismology, however, we are interested in the radiated seismic energy, which is the energy that flows out of the elastic body. The radiated seismic energy until a certain time t is

$$\begin{aligned} E_{\mathrm{s}}(t) &= -\int_0^t \mathrm{d}t \int_S \sigma_{ij}\dot{u}_i n_j \mathrm{d}S \\ &= -K(t) - \Delta U(t) + \int_0^t \mathrm{d}t \int_V f_i\dot{u}_i \mathrm{d}V \end{aligned} \qquad [13]$$

where $\Delta U(t)$ is the strain energy change inside the elastic body from time $t=0$ to t. If t is sufficiently long, so that all motion inside the body has ceased, $K(t) \to 0$ and we get the simplest possible expression

$$E_s = E_s(\infty) = -\Delta U + \int_0^\infty \mathrm{d}t \int_V f_i\dot{u}_i \mathrm{d}V \qquad [14]$$

Thus, total energy radiation is equal to the decrease in internal energy plus the work of the sources against the elastic deformation. Both terms in [14] contribute to seismic radiation as we will discuss in more detail for moment tensor sources and cracks.

Although we can use [14] to compute the seismic energy, it is easier to evaluate it directly from the first term in [13] assuming that S is very far from the source, so that far-field approximation [6] can be used in [13]. Consider, as shown in Figure 1, a cone of rays of cross section $\mathrm{d}\Omega$ issued from the source around the direction θ, ϕ. The energy crossing a section of this ray beam at distance R from the source per unit time is given by the energy

flow per unit solid angle $\dot{e}_s = \sigma_{ij}\dot{u}_i n_j R^2$, where σ_{ij} is the stress, $\dot{u}_i$ the particle velocity, and $\mathbf{n}$ the normal to the surface $\mathrm{d}S = R^2\mathrm{d}\Omega$. We now use [6] in order to compute σ_{ij} and $\dot{u}$. By straightforward differentiation and keeping only terms of order $1/R$ with distance, we get $\sigma_{ij}n_j \approx \rho c\dot{u}_i$ where ρc is the wave impedance and c the appropriate wave speed. The energy flow rate per unit solid angle for each type of wave is then

$$\dot{e}_s(t) = \rho c R^2 \dot{u}^2(R,t) \qquad [15]$$

Using the far-field approximation for the velocity derived from [6] and integrating around the source for the complete duration of the source, we get the total energy flow associated with P- and S-waves:

$$\begin{aligned} E_s^P &= \frac{1}{4\pi\rho\alpha^3}\left\langle R^P\right\rangle_2 \int_0^\infty s^{-2}(t)\mathrm{d}t \quad \text{for P waves} \\ E_s^S &= \frac{1}{4\pi\rho\beta^3}\left\langle \Re^S\right\rangle_2 \int_0^\infty s^{-2}(t)\mathrm{d}t \quad \text{for S waves} \end{aligned} \qquad [16]$$

where $\langle \Re^c\rangle_2 = 1/(4\pi)\int_\Omega (\Re^c)^2\mathrm{d}\Omega$ is the mean squared radiation pattern for wave $c = \{\mathrm{P},\mathrm{S}\}$. Since the radiation patterns are the simple sinusoidal functions listed in [7], the mean square radiation patterns are 1/3 for P-waves and 2/3 for the sum of the two components of S-waves. In [16], we assumed that $\dot{s}(t) = 0$ for $t < 0$. Finally, it is not difficult to verify that, since $\dot{s}$ has units of force rate, E_s and E_p have units of energy. Noting that in the Earth, α is roughly $\sqrt{3\beta}$ so that $\alpha^3 \cong 5\beta^3$; the amount of energy carried by the S-waves emitted by a point force of source time function $s(t)$ is close to ten times that carried by P-waves. For double-couple sources, this ratio is much larger.

4.02.2.5 The Green Tensor for a Point Force

The Green function is a tensor formed by the waves radiated from a set of three point forces aligned in the direction of each coordinate axis. For an arbitrary force of direction $\mathbf{f}$, located at point $\mathbf{x}_0$ and source function $s(t)$, we define the Green tensor for elastic waves by

$$\mathbf{u}(\mathbf{x},t) = G(\mathbf{x},t|\mathbf{x}_0,0)\cdot\mathbf{f} * s(t)$$

where the star indicates time-domain convolution.

We can also write this expression in the usual index notation

$$u_i(\mathbf{x},t) = \sum_j G_{ij}(\mathbf{x},t|\mathbf{x}_0,0) f_j * s(t)$$

in the time domain or

$$\widetilde{u}_i(\mathbf{x},\omega) = \sum_j \widetilde{G}_{ij}(\mathbf{x}|\mathbf{x}_0,\omega) f_j \widetilde{s}(\omega)$$

in the frequency domain.

The Green function itself can be easily obtained from the radiation from a point force [6]

$$\begin{aligned} G_{ij}(\mathbf{x},t|\mathbf{x}_0,0) = {} & \frac{1}{4\pi\rho}\left(\frac{1}{R}\right)_{,ij} t[\mathrm{H}(t-R/\alpha) - H(t-R/\beta)] \\ & + \frac{1}{4\pi\rho\alpha^2}\frac{1}{R}\left(R_{,i}R_{,j}\right)\delta(t-R/\alpha) \\ & + \frac{1}{4\pi\rho\beta^2}\frac{1}{R}\left[\delta_{ij} - R_{,i}R_{,j}\right]\delta(t-R/\beta) \end{aligned} \qquad [17]$$

Here, $\delta(t)$ is Dirac's delta, δ_{ij} is Kronecker's delta, and the comma indicates derivative with respect to the component that follows it.

Similarly, in the frequency domain,

$$\begin{aligned} \widetilde{G}_{ij}(\mathbf{x}|\mathbf{x}_0,\omega) = {} & \frac{1}{4\pi\rho}\left(\frac{1}{R}\right)_{,ij}\frac{1}{\omega^2}\left[-(1+i\omega R\alpha)\mathrm{e}^{-i\omega R/\alpha}\right. \\ & \left. + (1+i\omega R\beta)\mathrm{e}^{-i\omega R/\beta}\right] \\ & + \frac{1}{4\pi\rho\alpha^2}\frac{1}{R}\left(R_{,i}R_{,j}\right)\mathrm{e}^{-i\omega R/\alpha} \\ & + \frac{1}{4\pi\rho\beta^2}\frac{1}{R}\left[\delta_{ij} - R_{,i}R_{,j}\right]\mathrm{e}^{-i\omega R/\beta} \end{aligned}$$

4.02.3 Moment Tensor Sources

The Green function for a point force is the fundamental solution of the equation of elastodynamics. However – except for a few rare exceptions – seismic sources are due to fast internal deformation in the Earth, for instance, faulting or fast phase changes on localized volumes inside the Earth. For a seismic source to be of internal origin, it has to have zero net force and zero net moment. It is not difficult to imagine seismic sources that satisfy these two conditions:

$$\begin{aligned} \sum \mathbf{f} &= 0 \\ \sum \mathbf{f}\times\mathbf{r} &= 0 \end{aligned} \qquad [18]$$

The simplest such sources are dipoles and quadrupoles. For instance, the so-called linear dipole is made of two identical point forces of strength f that act in opposite directions at two points separated by a very small distance h along the axes of the forces. The seismic moment of this linear dipole is $M_0 = f\,h$. Experimental observation has shown that linear dipoles of this sort are not the most frequent models of seismic sources and, furthermore, there does not seem to be any simple internal deformation mechanism that corresponds to a pure linear dipole. It is possible to combine three orthogonal linear dipoles in order to form a general seismic source; any dipolar seismic source can be simulated by adjusting the strength of these three dipoles. It is obvious, as we will show later, that these three dipoles represent the principal directions of a symmetrical tensor of rank two that we call the seismic moment tensor:

$$\mathbf{M} = \begin{bmatrix} M_{xx} & M_{xy} & M_{xz} \\ M_{xy} & M_{yy} & M_{yz} \\ M_{xz} & M_{yz} & M_{zz} \end{bmatrix}$$

This moment tensor has a structure that is identical to that of a stress tensor, but it is not of elastic origin as we shall see promptly.

What do the off-diagonal elements of the moment tensor represent? Let us consider a moment tensor such that all elements are zero except M_{xy}. This moment tensor represents a double couple, a pair of two couples of forces that turn in opposite directions. The first of these couples consists in two forces of direction $\mathbf{e}_x$ separated by a very small distance h in the direction y. The other couple consists in two forces of direction $\mathbf{e}_y$ with a small arm in the direction x. The moment of each of

these couples is M_{xy}, the first pair has positive moment, and the second has a negative one. The conditions of conservation of total force and moment [18] are satisfied so that this source model is fully acceptable from a mechanical point of view. In fact, as shown by Burridge and Knopoff (1964), the double couple is the natural representation of a fault. One of the pair of forces is aligned with the fault, the forces indicate the directions of slip, and the arm is in the direction of the fault normal.

4.02.3.1 Radiation from a Point Moment Tensor Source

Let us now use the Green functions obtained for a point force in order to calculate the radiation from a point moment tensor source located at point $\mathbf{x}_0$:

$$\mathbf{M}_0(\mathbf{r}, t) = \mathbf{M}_0(t)\delta(\mathbf{x} - \mathbf{x}_0) \qquad [19]$$

$\mathbf{M}_0$ is the moment tensor, a symmetrical tensor whose components are independent functions of time.

We consider one of the components of the moment tensor, for instance, M_{ij}. This represents two point forces of direction i separated by an infinitesimal distance h_j in the direction j. The radiation of each of the point forces is given by the Green function G_{ij} computed in [17]. The radiation from the M_{ij} moment is then simply

$$u_k(\mathbf{x}, t) = \sum_{ij} G_{ki,j}(\mathbf{x}, t|\mathbf{x}_0, t) * M_{ij}(t) \qquad [20]$$

The complete expression of the radiation from a point moment tensor source can then be obtained from [17]. We will be interested only on the far-field terms since the near field is too complex to discuss here. We get for the far-field waves

$$\begin{aligned} u_i^{\mathrm{P}}(R, t) &= \frac{1}{4\pi\rho\alpha^3}\frac{1}{R}\sum_{jk}\mathfrak{R}_{ijk}^{\mathrm{P}}\dot{M}_{jk}(t - R/\alpha) \\ u_i^{\mathrm{S}}(R, t) &= \frac{1}{4\pi\rho\beta^3}\frac{1}{R}\sum_{jk}\mathfrak{R}_{ijk}^{\mathrm{S}}\dot{M}_{jk}(t - R/\beta) \end{aligned} \qquad [21]$$

where $\mathfrak{R}_{ijk}^{\mathrm{P}} = R_i R_j R_k$ and $\mathfrak{R}_{ijk}^{\mathrm{S}} = (\delta_{ij} - R_i R_j)R_k$ are the radiation patterns of P- and S-waves, respectively. We observe in [21] that the far-field signal carried by both P- and S-waves is the time derivative of the seismic moment components, so that far-field seismic waves are proportional to the moment rate of the source.

Very often in seismology, it is assumed that the geometry of the source can be separated from its time variation, so that the moment tensor can be written in the simpler form

$$\mathbf{M}_0(t) = \mathbf{M}\, s(t)$$

where $\mathbf{M}$ is a time-invariant tensor that describes the geometry of the source and $s(t)$ is the time variation of the moment, the source time function determined by seismologists. Referring to Figure 2, we can now write a simpler form of [21]

$$u^{\mathrm{c}}(\mathbf{x}, t) = \frac{1}{4\pi\rho c^3}\frac{\mathfrak{R}^{\mathrm{c}}(\theta, \phi)}{R}\Omega(t - R/c) \qquad [22]$$

where R is the distance from the source to the observer. c stands for either α for P-waves or β for shear waves (SH and SV). For P-waves, u^c is the radial component; for S-waves, it is the appropriate transverse component for SH or SV waves. In

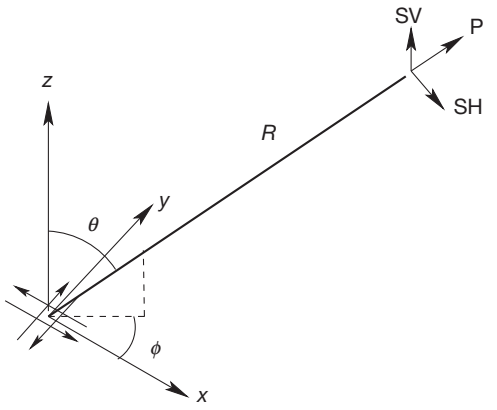

Figure 2 Radiation from a point double source. The source is at the origin and the observer at a position defined by the spherical coordinates R, θ, ϕ, distance, polar angle, and azimuth.

[22], we have introduced the standard notation $\Omega(t) = \dot{s}(t)$ for the source time function, the signal emitted by the source in the far field.

The term $\mathfrak{R}^{\mathrm{c}}(\theta, \phi)$ is the radiation pattern, a function of the takeoff angle of the ray at the source. Let (R, θ, ϕ) be the radius, colatitude, and azimuth of a system of spherical coordinates centered at the source, respectively. It is not difficult to show that the radiation pattern is given by

$$\mathfrak{R}^{\mathrm{c}}(\theta, \phi) = \mathbf{e}_{\mathrm{R}} \cdot \mathbf{M} \cdot \mathbf{e}_{\mathrm{R}} \qquad [23]$$

for P-waves, where $\mathbf{e}_{\mathrm{R}}$ is the radial unit vector at the source. Assuming that the z-axis at the source is vertical, so that θ is measured from that axis, S-waves are given by

$$\mathfrak{R}^{\mathrm{SV}}(\theta, \phi) = \mathbf{e}_\theta \cdot \mathbf{M} \cdot \mathbf{e}_{\mathrm{R}} \quad \text{and} \quad \mathfrak{R}^{\mathrm{SH}}(\theta, \phi) = \mathbf{e}_\phi \cdot \mathbf{M} \cdot \mathbf{e}_{\mathrm{R}} \qquad [24]$$

where $\mathbf{e}_\phi$ and $\mathbf{e}_\theta$ are unit vectors in spherical coordinates. Thus, the radiation patterns are the radial components of the moment tensor projected on spherical coordinates.

With minor changes to take into account smooth variations of elastic wave speeds in the Earth, these expressions are widely used to generate synthetic seismograms in the so-called far-field approximation. The main changes that are needed are the use of travel time $T_{\mathrm{c}}(r, r_{\mathrm{o}})$ instead of R/c in the waveform $\Omega(t - T_{\mathrm{c}})$ and a more accurate geometric spreading factor $g(\Delta, H)/a$ to replace $1/R$, where a is the radius of the Earth and $g(\Delta, H)$ is a tabulated function that depends on the angular distance Δ between the hypocenter and the observer and the source depth H. In most work with local earthquakes, the approximation [22] is frequently used with a simple correction for free surface response.

4.02.3.2 A More General View of Moment Tensors

What does a seismic moment represent? A number of mechanical interpretations are possible. In the previous sections, we introduced it as a simple mechanical model of double couples and linear dipoles. Other authors Eshelby (1956) and Backus and Mulcahy (1976) have explained them in terms of the distribution of inelastic stresses (sometimes called stress 'glut').

Let us first notice that a very general distribution of force that satisfies the two conditions [18] necessarily derives from a symmetrical seismic moment density of the form

$$\mathbf{f}(\mathbf{x}, t) = \nabla \cdot \mathbf{M}(\mathbf{x}, t) \qquad [25]$$

where $\mathbf{M}(\mathbf{x}, t)$ is the moment tensor density per unit volume. Gauss' theorem can be used to prove that such a force distribution has no net force nor moment. In many areas of applied mathematics, the seismic moment distribution is often termed a 'double layer potential.'

We can now use [25] in order to rewrite the elastodynamic eqn [1] as a system of first-order partial differential equations:

$$\begin{aligned} \rho \frac{\partial}{\partial t}\mathbf{v} &= \nabla \cdot \sigma \\ \frac{\partial}{\partial t}\sigma &= \lambda \nabla \cdot \mathbf{v}\mathbf{I} + \mu\left[(\nabla \mathbf{v}) + (\nabla \mathbf{v})^{\mathrm{T}}\right] + \dot{\mathbf{M}}_0 \end{aligned} \qquad [26]$$

where $\mathbf{v}$ is the particle velocity and σ is the corresponding elastic stress tensor. We observe that the moment tensor density source appears as an addition to the elastic stress rate $\dot{\sigma}$. This is probably the reason that Backus and Mulcahy (1976) adopted the term 'glut.' In many other areas of mechanics, the moment tensor is considered to represent the stresses produced by inelastic processes. A full theory of these stresses was proposed by Eshelby (1956). Incidentally, the equation of motion written in this form is the basis of some very successful numerical methods for the computation of seismic wave propagation see, for example, Madariaga (1976), Virieux (1986), and Madariaga et al. (1998).

We can get an even clearer view of the origin of the moment tensor density by considering it as defining an *inelastic* strain tensor ε^{I} defined implicitly by

$$(m_0)_{ij} = \lambda \delta_{ij} \varepsilon^{\mathrm{I}}_{kk} + 2\mu \varepsilon^{\mathrm{I}}_{ij} \qquad [27]$$

Many seismologists have tried to use ε_{I} in order to represent seismic sources. Sometimes termed 'potency' (Ben Menahem and Singh, 1981), the inelastic strain has not been widely adopted even if it is a more natural way of introducing seismic source in bimaterial interfaces and other heterogeneous media. For a recent discussion, see Ampuero and Dahlen (2005).

The meaning of ε^{I} can be clarified by reference to **Figure 3**. Let us make the following 'gedanken'experiment. Let us cut an infinitesimal volume V from the source region. Next, we let it undergo some inelastic strain ε^{I}, for instance, a shear strain due to the development of internal dislocations as shown in the figure. Let us now apply stresses on the borders of the internally deformed volume V so as to bring it back to its original shape. If the elastic constants of the internally deformed volume V have not changed, the stresses needed to bring V back to its original shape are exactly given by the moment tensor components defined in [27]. This is the definition of seismic moment tensor: It is the stress produced by the inelastic deformation of a body that is elastic everywhere. It should be clear that the moment tensor is not the same thing as the stress tensor acting on the fault zone. The latter includes the elastic response to the introduction of internal stresses as shown in the last row of **Figure 3**. The difference between the initial stresses before the internal deformation and those that prevail after the deformed body has been reinserted in the elastic medium is the stress change (or stress drop as originally introduced in seismology in the late 1960s). If the internal strain is produced in the sense of reducing applied stress – and reducing internal strain energy – then stresses inside the source will decrease in a certain average sense. It must be understood, however, that a source of internal origin – like faulting – can only redistribute internal stresses. During faulting, stresses reduce in the immediate vicinity of slip zones but increase almost everywhere else.

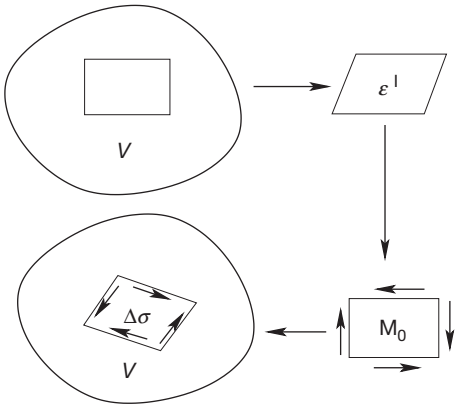

Figure 3 Inelastic stresses or stress glut at the origin of the concept of seismic moment tensor. We consider a small rectangular zone that undergoes a spontaneous internal deformation ϵ^{I} (top row). The elastic stresses needed to bring it back to a rectangular shape are the moment tensor or stress glut (bottom row right). Once stresses are relaxed by interaction with the surrounding elastic medium, the stress change is $\Delta\sigma$ (bottom left).

4.02.3.3 Moment Tensor Equivalent of a Fault

For a point moment tensor of type [27], we can write

$$(M_0)_{ij} = \left(\lambda \delta_{ij} \varepsilon^{\mathrm{I}}_{kk} + 2\mu \varepsilon^{\mathrm{I}}_{ij}\right) V \delta(\mathbf{x} - \mathbf{x}_0) \qquad [28]$$

where V is the elementary source volume on which acts the source. Let us now consider that the source is a very thin cylinder of surface S, thickness h, volume $V = Sh$, and unit normal $\mathbf{n}$. Letting the thickness of the cylinder tend to zero, the mean inelastic strain inside the volume V can be computed as follows:

$$\lim_{h \to 0} \varepsilon^{\mathrm{I}}_{ij} h = \frac{1}{2}\left[\Delta u_i n_j + \Delta u_j n_i\right] \qquad [29]$$

where Δu is the displacement discontinuity (or simply the *slip*) across the fault volume. The seismic moment for the flat fault is then

$$(M_0)_{ij} = \left[\lambda \delta_{ij} \Delta u_k n_k + \mu\left(\Delta u_i n_j + \Delta u_j n_i\right)\right] S \qquad [30]$$

so that the seismic moment can be defined for a fault as the product of an elastic constant with the displacement discontinuity and the source area. Actually, this is the way the seismic moment was originally determined by Burridge and Knopoff (1964). If the slip discontinuity is written in terms of a direction of slip v and a scalar slip D, $\Delta u_i = D v_i$, we get

$$(M_0)_{ij} = \delta_{ij} v_k n_k \lambda D S + \left(v_i n_j + v_j n_i\right) \mu D S \qquad [31]$$

Most seismic sources do not produce normal displacement discontinuities (fault opening) so that $v \cdot \mathbf{n} = 0$ and the first

term in [30] is equal to zero. In that case, the seismic moment tensor can be written as the product of a tensor with the scalar seismic moment $M_0 = \mu DS$:

$$(M_0)_{ij} = (v_i n_j + v_j n_i)\mu DS \qquad [32]$$

The first practical determination of the scalar seismic moment is due to Aki (1966), who estimated M_0 from seismic data recorded after the Niigata earthquake of 1966 in Japan. Determination of seismic moment has become the standard way in which earthquakes are measured. All sorts of seismological, geodetic, and geologic techniques have been used to determine M_0. A worldwide catalog of seismic moment tensors was made available online by Harvard University (Dziewonski and Woodhouse, 1983). Initially, moments were determined by for the limited form [32], but nowadays, the full set of six components of the moment tensor is regularly computed.

Let us remark that the restricted form of the moment tensor [32] reduces the number of independent parameters of the moment tensor from 6 to 4. Very often, seismologists use the simple fault model of the source moment tensor. In practice, the fault is parameterized by the seismic moment plus the three Euler angles of the fault plane. Following the convention adopted by Aki and Richards (2002), these angles are defined as δ the dip of the fault, ϕ the strike of the fault with respect to the north, and λ the rake of the fault, which is the angle of the slip vector with respect to the horizontal.

4.02.3.4 Eigenvalues and Eigenvectors of the Moment Tensor

Since the moment tensor is a symmetrical tensor of order 3, it has three orthogonal eigenvectors with real eigenvalues, just like any stress tensor. These eigenvalues and eigenvectors are the three solutions of

$$\mathbf{M}_0\mathbf{v} = m\mathbf{v}$$

Let the eigenvalues and eigenvector be

$$m_i, \quad \mathbf{v}_i \qquad [33]$$

Then, the moment tensor can be rewritten as

$$\mathbf{M}_0 = \sum_i m_i \mathbf{v}_i^{\mathrm{T}} \mathbf{v}_i \qquad [34]$$

Each eigenvalue–eigenvector pair represents a linear dipole. The eigenvalue represents the moment of the dipole. From extensive studies of moment tensor sources, it appears that many seismic sources are very well represented by an almost pure double-couple model with $m_1 = -m_3$ and $m_2 \cong 0$.

A great effort for calculating moment tensors for deeper sources has been made by several authors in recent years. It appears that the non-double couple part is larger for these sources but that it does not dominate the radiation. For deep sources, Knopoff and Randall (1970) proposed the so-called compensated linear vector dipole (CLVD). This is a simple linear dipole from which we subtract the volumetric part so that $m_1 + m_2 + m_3 = 0$. Thus, a CLVD is a source model where $m_2 = m_3 = -1/2 m_1$. Radiation from a CLVD is very different from that from a double-couple model, and many seismologists have tried to separate a double couple from CLVD components from the moment tensor. In fact, moment tensors are better represented by their eigenvalues; separation into a fault and a CLVD part is generally ambiguous.

Seismic moments are measured in units of Nm. Small earthquakes that produce no damage have seismic moments less than 10^{12} Nm, while the largest subduction events, like those of Chile in 1960, Alaska in 1964, and Sumatra in 2004, have moments of the order of 10^{22}–10^{23} Nm. Large destructive events like Izmit, Turkey, 1999; Chichi, Taiwan, 1999; and Landers, California, 1992 have moments of the order of 10^{20} Nm.

Since the late 1930s, it became commonplace to measure earthquakes by their magnitude, a logarithmic measure of the total energy radiated by the earthquake. Methods for measuring radiated energy were developed by Gutenberg and Richter using well-calibrated seismic stations. At the time, the general properties of the radiated spectrum were not known and the concept of moment tensor had not yet been developed. Since at present time earthquakes are systematically measured using seismic moments, it has become standard to use the following empirical relation defined by Kanamori (1977) and Hanks and Kanamori (1979) to convert moment tensors into a magnitude scale:

$$\log_{10} M_0 \quad (\text{in Nm}) \quad = 1.5 M_w + 9 \qquad [35]$$

Magnitudes are easier to retain and have a clearer meaning for the general public than the more difficult concept of moment tensor.

4.02.3.5 Seismic Radiation from Moment Tensor Sources in the Spectral Domain

In actual applications, the near-field signals radiated by earthquakes may become quite complex because of multipathing, scattering, etc., so that the actually observed seismogram, say, $u(t)$, resembles the source time function $\Omega(t)$ only at long periods. It is usually verified that complexities in the wave propagation affect much less the spectral amplitudes in the Fourier transformed domain. Radiation from a simple point moment tensor source can be obtained from [22] by straightforward Fourier transformation:

$$\tilde{u}_c(\mathbf{x}, \omega) = \frac{1}{4\pi\rho c^3} \frac{\Re^c(\theta_0, \phi_0)}{R} \tilde{\Omega}(\omega) e^{-i\omega R/c} \qquad [36]$$

where $\tilde{\Omega}(\omega)$ is the Fourier transform of the source time function $\Omega(t)$. A well-known property of Fourier transform is that the low-frequency limit of the transform is the integral of the source time function, that is,

$$\lim_{\omega \to 0} \tilde{\Omega}(\omega) = \int_0^\infty \dot{M}_0(t) \mathrm{d}t = M_0$$

So that in fact, the low-frequency limit of the transform of the displacement yields the total moment of the source. Unfortunately, the same notation is used to designate the total moment release by an earthquake – M_0 – and the time-dependent moment $M_0(t)$.

From the observation of many earthquake spectra, and from the scaling of moment with earthquake size, Aki (1967) and Brune (1970) concluded that the seismic spectra decayed as ω^{-2} at high frequencies. Although, in general, spectra are more complex for individual earthquakes, a simple source model can be written as follows:

$$\Omega(\omega) = \frac{M_0}{1 + (\omega/\omega_0)^2} \quad [37]$$

where ω_0 is the so-called corner frequency. In this simple 'omega-squared model,' seismic sources are characterized by only two independent scalar parameters: the seismic moment M_0 and the corner frequency ω_0. Not all earthquakes have displacement spectra as simple as [37], but the omega-squared model is a convenient starting point for understanding seismic radiation.

From [37], it is possible to compute the spectra of ground velocity $\dot{\Omega}(\omega) = i\omega\Omega(\omega)$. Ground velocity spectra have a peak situated roughly at the corner frequency ω_0. In actual earthquake spectra, this peak is usually broadened and contains oscillations and secondary peaks; at higher frequencies, attenuation, propagation scattering, and source effects reduce the velocity spectrum.

Finally, by an additional differentiation, we get the acceleration spectra $\ddot{\Omega}(\omega) = -\omega^2\Omega(\omega)$. This spectrum has an obvious problem; it predicts that ground acceleration is flat for arbitrarily high frequencies. The acceleration spectrum usually decays after a high-frequency corner identified as f_{max}. The origin of this high-frequency cutoff was a subject of discussion in the 1990s, which was settled by the implicit agreement that f_{max} reflects the dissipation of high-frequency waves due to propagation in a strongly scattering medium, like the crust and near-surface sediments.

It is interesting to observe that [37] is the Fourier transform of

$$\Omega(t) = \frac{M_0\omega_0}{2} e^{-|\omega_0 t|} \quad [38]$$

This is a noncausal strictly positive function, is symmetrical about the origin, and has an approximate width of $1/\omega_0$. By definition, the integral of the function is exactly equal to M_0. Even if this function is noncausal, it shows that $1/\omega_0$ controls the width or duration of the seismic signal. At high frequencies, the function behaves like ω^{-2}. This is due to the slope discontinuity of [38] at the origin.

We can also interpret [37] as the absolute spectral amplitude of a causal function. There are many such functions, one of them – proposed by Brune (1970) – is

$$\Omega(t) = M_0\omega_0^2 t\, e^{-\omega_0 t} H(t) \quad [39]$$

As for [38], the width of the function is roughly $1/\omega_0$ and the high frequencies are due to the slope break of $\Omega(t)$ at the origin. This slope break has the same amplitude as that of [38].

4.02.3.6 Seismic Energy Radiated by Point Moment Tensor Sources

In Section 4.02.2.4, we discussed the general energy balance for a seismic source embedded in an elastic medium. The energy flow for a moment tensor source can be derived from expression [14], where we replace the force density by its expression in terms of a moment density [25]. After a few small changes and integration by parts, we get

$$E_s = -\Delta U + \int_0^\infty dt \int_V M_{ij}\dot{\varepsilon}_{ij} dV \quad [40]$$

Seismic radiation is equal to the reduction in internal strain energy plus the work of the moment tensor against the elastic strain rate at the source.

As we have already discussed for a point force, at any position sufficiently far from the source, energy flow per unit solid angle is proportional to the square of local velocity [15]. Using the far-field approximation [36], we can follow the same steps as in [16] to express the radiated energy in terms of the seismic source time function as

$$E_c = \frac{1}{4\pi\rho c^5}\langle \Re^c \rangle_2 \int_0^\infty \dot{\Omega}^2(t) dt$$

where c stands again for P- or S-waves and, as in [18], $\langle \Re^i \rangle_2 = 1/(4\pi)\int_\Omega (\Re^i)^2 d\Omega$ is the mean square radiation pattern. We can now use Parseval's theorem

$$\int_0^\infty \dot{\Omega}(t)^2 dt = \frac{1}{\pi}\int_0^\infty \omega^2 \widetilde{\Omega}(\omega)^2 d\omega$$

in order to express the radiated energy in terms of the seismic spectrum as

$$E_c = \frac{1}{4\pi^2\rho c^5}\langle \Re^c \rangle_2 \int_0^\infty \omega^2\Omega^2(\omega) d\omega \quad [41]$$

For Brune's spectrum [37], the integral is

$$\int_0^\infty \omega^2\Omega^2(\omega) d\omega = \frac{\pi}{2} M_0^2\omega_0^3$$

so that radiated energy is proportional to the square of moment. We can finally write

$$\frac{E_c}{M_0} = \frac{1}{16\pi\rho c^5}\langle \Re^c \rangle^2 M_0\omega_0^3 \quad [42]$$

This nondimensional relation makes no assumptions about the rupture process at the source except that the spectrum is of the form [37]. Noting that in the Earth, α is roughly $\sqrt{3}\beta$ so that $\alpha^5 \cong 16\beta^5$, the amount of energy carried by the S-waves emitted by a point moment tensor is close to 25 times that carried by P-waves, if the source spectrum is the same for P- and S-waves. For finite sources, the partition of energy into P- and S-waves depends on the details of the rupture process.

Since the energy flow e_c can usually be determined in only a few directions, (θ, ϕ) of the focal sphere, the energy-moment ratio [42] can only be estimated, never computed very precisely. This problem still persists; in spite of the deployment of increasingly denser instrumental networks, there will always be large areas of the focal sphere that remain out of the domain of seismic observations because the waves in those directions are refracted away from the station networks, energy is dissipated due to long trajectories, etc.

4.02.3.7 More Realistic Radiation Models

In reality, earthquakes occur in a complex medium that is usually scattering and dissipative. Seismic waves become diffracted and reflected and in general suffer multipathing in those structures. Accurate seismic modeling would require perfect knowledge of those structures. It is well known and understood that those complexities dominate signals in certain frequency bands. For this reason, the simple model presented

here can be used to understand many features of earthquakes, and the more sophisticated approaches that attempt to model every detail of the waveform are reserved only for more advanced studies. Here, like in many other areas of geophysics, a balance between simplicity and concepts must be kept against numerical complexity that may not always be warranted by lack of knowledge of the details of the structures. If the simple approach were not possible, then many standard methods to study earthquakes would be impossible to use. For instance, source mechanism, the determination of the fault angles δ, ϕ, and λ, would be impossible. These essential parameters are determined by back projection of the displacement directions from the observer to a virtual unit sphere around the point source.

A good balance between simple, but robust concepts, and the sophisticated reproduction of the complex details of real wave propagation is a permanent challenge for seismologists. Nowadays, numerical techniques become more and more common. Our simple models detailed earlier are not to be easily neglected; in any case, they should always serve as test models for fully numerical methods.

4.02.4 Finite Source Models

The point source model we just discussed provides a simple approach to the simulation of seismic radiation. It is probably quite sufficient for the purpose of modeling small sources situated sufficiently far from the observer so that the source looks like a single point source. Details of the rupture process are then hidden inside the moment tensor source time function $M_0(t)$. For larger earthquakes, and especially for earthquakes observed at distances close to the source, the point source model is not sufficient, and one has to take into account the geometry of the source and the propagation of rupture across the fault. Although the first finite models of the source are quite ancient, their widespread use to model earthquakes is relatively recent and has been more extensively developed as the need to understand rupture in detail has been more pressing. The first models of a finite fault were developed simultaneously by Maruyama (1963) and Burridge and Knopoff (1964) in the general case, by Ben Menahem (1961, 1962) for surface and body waves, and by Haskell (1964, 1966) who provided a very simple solution for the far field of a rectangular fault. Haskell's model became the *de facto* earthquake fault model in the late 1960s and early 1970s and was used to model many earthquakes. In the following, we review the available finite source models, focusing on the two main models: the rectangular fault and the circular fault.

4.02.4.1 The Kinematic Dislocation Model

In spite of much recent progress in understanding the dynamics of earthquake ruptures, the most widely used models for interpreting seismic radiation are the so-called dislocation models. In these models, the earthquake is simulated as the kinematic spreading of a displacement discontinuity (slip or dislocation in seismological usage) along a fault plane. As long as the thickness of the fault zone H is negligible with respect to the other length scales of the fault (width W and length L), the fault may be idealized as a surface of displacement discontinuity or slip. Slip is very often called dislocation by seismologists, although this is not the same as the concept of a dislocation in solid mechanics.

In its most general version, slip as a function of time and position in a dislocation model is completely arbitrary, and rupture propagation may be as general as wanted. In this version, the dislocation model is an appropriate description of an earthquake as the propagation of a slip episode on a fault plane. It must be remarked, however, that not all slip distributions are physically acceptable. Madariaga (1978) showed that Haskell's model, by far the most used dislocation model, presents unacceptable features like interpenetration of matter that make it very difficult to use at high frequencies without important modifications. The most serious problem with Haskell's model is that strain energy release is infinite, so that this model is not useful for the study of seismic energy balance. For this reason, dislocation models must be considered as an intermediate step in the formulation of a physically acceptable description of rupture but examined critically when converted into dynamic models. From this perspective, dislocation models are very useful step in the inversion of near-field accelerograms (see, e.g., Wald and Heaton, 1994).

A finite source model can be described as a distribution of moment tensor sources. Since we are interested in radiation from faults, we use the approximation [32] for the moment of a fault element. Each of these elementary sources produces a seismic radiation that can be computed using the Green function [17]. The total displacement seismogram observed at an arbitrary position $\mathbf{x}$ is the sum

$$u_i(\mathbf{x}, t) = \int_0^t \int_S \mu(\mathbf{x}_0) \Delta u_j(\mathbf{x}_0, \tau) G_{ij,k}(\mathbf{x}, t|\mathbf{x}_0, \tau) n_k(\mathbf{x}_0) \mathrm{d}^2\mathbf{x}_0 \mathrm{d}\tau \quad [43]$$

where $\Delta u(\mathbf{x}_0, t)$ is the slip across the fault of surface S as a function of position on the fault ($\mathbf{x}_0$) and time t. $\mathbf{n}$ is the normal to the fault and $\mathbf{G}(x, t)$ is the elastodynamic Green tensor that may be computed using simple layered models of the crustal structure or more complex finite difference simulations.

In a first, simple analysis, we can use the far-field approximation [22] that is often used to generate synthetic seismograms far from the source (see, e.g., Kikuchi and Kanamori, 1982, 1991). Inserting [22] into [43] and after some simplification, we get

$$u^c(\mathbf{x}, t) = \frac{1}{4\pi\rho c^3} \int_0^t \int_S \frac{\mathfrak{R}^c_{ijk}(\theta, \phi)}{R} \mu \Delta \dot{u}_j \left[\mathbf{x}_0, t - \tau - \frac{R(\mathbf{x} - \mathbf{x}_0)}{c}\right] n_k \mathrm{d}^2\mathbf{x}_0 \mathrm{d}\tau \quad [44]$$

where $R(\mathbf{x} - \mathbf{x}_0)$ is the distance between the observer and a source point located at $\mathbf{x}_0$. In almost all applications, the reference point is the hypocenter, the point where rupture initiates.

In [44], both the radiation pattern $\mathfrak{R}^c$ and the geometric decay $1/R$ change with position on the fault. In the far field, according to ray theory, we can make the approximation that only travel time changes are important so that we can approximate the integral [44] assuming that both radiation pattern and geometric spreading do not change significantly over the fault. In the far field, we can also make the so-called Fraunhofer approximation:

$$R(\mathbf{x}-\mathbf{x}_0)\cong R(\mathbf{x}-\mathbf{x}_H)-\mathbf{e}_r\cdot(\mathbf{x}_0-\mathbf{x}_H)$$

where $\mathbf{x}_H$ is a reference point on the fault, usually the hypocenter, and $\mathbf{e}_r$ is the unit vector in the radial direction from the reference point to the observer. With these approximations, far-field radiation from a finite source is again given by the generic expression [22] where the source time function Ω is replaced by

$$\Omega(t,\theta,\phi)=\mu\int_0^t\int_S \Delta\dot{u}_j\left[\xi_1,\xi_2,t-\tau+\frac{\mathbf{e}_r\cdot\xi}{c}\right]d\xi_1 d\xi_2 d\tau \qquad [45]$$

where ξ is a vector of component (ξ_1,ξ_2) that measures position on the fault with respect to the hypocenter $\mathbf{x}_H$. The main difference between a point and a finite source as observed from the far field is that in the finite case, the source time function Ω depends on the direction of radiation (θ,ϕ) through the term $\mathbf{e}_r\cdot\xi$. This directivity of seismic radiation can be very large when ruptures propagate at high subshear or intersonic speeds (**Chapter 4.09**).

The source time function expression [45] is linear in slip rate amplitude but very nonlinear with respect to rupture propagation, which is implicit in the time dependence of $\Delta\dot{u}$. For this reason, in most inversions, the kinematics of the rupture process (position of rupture front as a function of time) is simplified. The most common assumption is to assume that rupture propagates at constant speed away from the hypocenter. Different approaches have been proposed in the literature in order to approximately invert for variations in rupture speed about the assumed constant rupture velocity (see, e.g., Cotton and Campillo, 1995; Hartzell and Heaton, 1983; Wald and Heaton, 1994; **Chapter 4.09**).

4.02.4.1.1 Haskell's rectangular fault model

One of the most widely used dislocation model was introduced by Haskell (1964, 1966). In this model, shown in **Figure 4**, a uniform displacement discontinuity spreads at constant rupture velocity inside a rectangular-shaped fault. Although from a mechanical point of view this model violates simple principles of continuum mechanics, like continuity of matter, it is a very useful first approximation to a seismic source. At low frequencies, or wavelengths much longer than the size of the fault, this model is a reasonable approximation to a simple seismic rupture propagating along a strike-slip fault.

In Haskell's model, at time $t=0$, a line of dislocation of width W appears suddenly and propagates along the fault at a constant rupture velocity until a region of length L of the fault has been broken. As the dislocation moves, it leaves behind a zone of constant slip D. Assuming that the fault lies on a plane of coordinates (ξ_1,ξ_2), the slip function can be written as (see also **Figure 4**)

$$\Delta\dot{u}_1(\xi_1,\xi_2,t)=D\dot{s}(t-\xi_1/v_r)H(\xi_1)H(L-\xi_1)$$
$$\text{for}\quad -W/2<\xi_2<W/2 \qquad [46]$$

where $\dot{s}(t)$ is the slip rate time function that in the simplest version of Haskell's model is invariant with position on the fault. The most important feature of this model is the propagation of rupture implicit in the time delay of rupture. $\xi_1/v_r\cdot v_r$ is the rupture velocity, the speed with which the slip front propagates along the fault in the ξ_1 direction. An obvious unphysical feature of this model is that rupture appears instantaneously in the ξ_2 direction, this is of course impossible for a spontaneous seismic rupture. The other inadmissible feature of Haskell's model is the fact that on its borders, slip suddenly jumps from the average slip D to zero. This violates material continuity so that the most basic equation of motion (1) is no longer valid near the edges of the fault. In spite of these two obvious shortcomings, Haskell's model gives a simple, first-order approximation to seismic slip, fault finiteness at a finite rupture speed. The seismic moment of Haskell's model is easy to compute, the fault area is $L\times W$, and slip D is constant over the fault, so that the seismic moment is $M_0=\mu DLW$. Using the far-field approximation, we can compute the source time function for Haskell's model:

$$\Omega_H(t,\theta,\phi)=\mu\int_{-W/2}^{W/2}d\xi_2\int_0^L D\dot{s}\left[t-\frac{\xi_1}{v_r}+\frac{\xi_1}{c}\cos\phi\sin\theta+\frac{\xi_2}{c}\sin\phi\sin\theta\right]d\xi_1 \qquad [47]$$

where we used the index H to indicate that this is Haskell's model. The two integrals can be evaluated very easily for an observer situated along the axis of the fault, that is, when $\phi=0$.

Integrating, we get

$$\Omega_H(\theta,0,t)=M_0\frac{1}{T_M}\int_0^{\min(t,T_M)}\dot{s}(t-\tau)d\tau \qquad [48]$$

where $T_M=L/c(1-v_r/c\sin\theta)$. Thus, the far-field signal is a simple integral over time of the source slip rate function. In other directions, the source time function Ω_H is more complex, but it can be easily computed by the method of isochrones that we will explain shortly. Radiation from Haskell's model shows two very fundamental properties of seismic radiation: finite duration given by T_M and directivity, that is, the duration and amplitude of seismic waves depend on the radiation angles θ and ϕ.

A similar computation in the frequency domain was made by Haskell (1966) for the particular direction $\phi=0$. In our notation, the result is

$$\tilde{\Omega}_H(\theta,0,\omega)=M_0\mathrm{sinc}(\omega T_M/2)e^{-i\omega T_M/2}\tilde{\dot{s}}(\omega) \qquad [49]$$

where $\mathrm{sinc}(x)=sin(x)/x$.

It is often assumed that the slip rate time function $\dot{s}(t)$ is a boxcar function of amplitude $1/\tau_r$ and duration τ_r, the rise time. In that case, the spectrum $\tilde{\Omega}(\omega)$ becomes

$$\tilde{\Omega}_H(\theta,0,\omega)=M_0\mathrm{sinc}(\omega T_M/2)\mathrm{sinc}(\omega\tau_r/2)e^{-i\omega(T_M+\tau_r)/2} \qquad [50]$$

or in the time domain

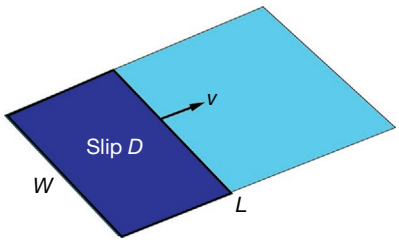

Figure 4 Haskell's kinematic model, one of the simplest possible earthquake models. The fault has a rectangular shape, and a linear rupture front propagates from one end of the fault to the other at constant rupture speed v. Slip in the broken part of the fault is uniform and equal to D.

$$\Omega_H(\theta, 0, t) = M_0 \text{boxcar}[t, T_M] * \text{boxcar}[t, \tau_r]$$

where the star means convolution and boxcar is a function of unit area that is zero everywhere except that in the time interval from 0 to τ_r where it is equal to $1/\tau_r$. Thus, Ω_H is a simple trapezoidal pulse of area M_0 and duration $T_d = T_M + \tau_r$. This surprisingly simple source time function matches the ω-squared model for the far-field spectrum since Ω_H is flat at low frequencies and decays like ω^{-2} at high frequencies. The spectrum has two corners associated with the pulse duration T_M and the other with rise time τ_r. This is unfortunately only valid for radiation along the plane $\phi = 0$ or $\phi = \pi$. In other directions with $\phi \neq 0$, radiation is more complex and the high-frequency decay is of order ω^{-3}, faster than in classical Brune's model.

In spite of some obvious mechanical shortcomings, Haskell's model captures some of the most important features of an earthquake and has been extensively used to invert for seismic source parameters in both the near field and far field from seismic and geodetic data. The complete seismic radiation for Haskell's model was computed by Madariaga (1978).

4.02.4.2 The Circular Fault Model

The other simple source model that has been widely used in earthquake source seismology is a circular crack model. This model was introduced by several authors including Savage (1966), Brune (1970), and Keylis-Borok (1959) to quantify a simple source model that was mechanically acceptable and to relate slip on a fault to stress changes. As we have already mentioned, dislocations models like Haskell's produce nonintegrable stress changes due to the violation of material continuity at the edges of the fault. The circular crack model was a natural approach to model earthquakes avoiding nonphysical singularities. In the present section, we will examine the circular crack model from a kinematic point of view.

4.02.4.2.1 Kostrov's self-similar circular crack

The simplest possible crack model is that of a circular rupture that starts from a point and then spreads self-similarly at constant rupture speed v_r without ever stopping. Slip on this fault is driven by stress drop inside the fault. The solution of this problem is somewhat difficult to obtain because it requires very advanced use of self-similar solutions to the wave equation and its complete solution for displacements and stresses must be computed using the Cagniard–de Hoop method (Richards, 1976). Fortunately, the solution for slip across the fault found by Kostrov (1964) is surprisingly simple:

$$\Delta u_x(r, t) = C(v_r)\frac{\Delta\sigma}{\mu}\sqrt{v_r^2 t^2 - r^2} \qquad [51]$$

where r is the radius in a cylindrical coordinate system centered on the point of rupture initiation (see **Figure 5**). $V_r t$ is the instantaneous radius of the rupture at time t. $\Delta\sigma$ is the constant stress drop inside the rupture zone, μ is the elastic rigidity, and $C(v_r)$ is a very slowly varying function of the rupture velocity. For most practical purposes, $C \approx 1$. As shown by Kostrov (1964), inside the fault, the stress change produced by the slip function [51] is constant and equal to $\Delta\sigma$. This simple solution provides a very basic result that is one of the most important properties of circular cracks. Slip in the fault scales with the ratio of stress drop over rigidity times the instantaneous radius of the fault. As rupture radius increases, all the displacements around the fault scale with the size of the rupture zone.

The circular self-similar rupture model produces far-field seismic radiation with a very peculiar signature. Inserting the slip function into the expression for far-field radiation [45], we get

$$\Omega_K(t, \theta) = A(v_r, \theta) t^2 H(t)$$

where we used an index K to indicate Kostrov's model. The amplitude coefficient A is

$$A(v_r, \theta) = C(v_r)\frac{2\pi}{\left(1 - v_r^2/c^2 \sin^2\theta\right)^2}\Delta\sigma v_r^3$$

(see Boatwright, 1980; Richards, 1976). Thus, the initial rise of the far-field source time function is proportional to t^2 for Kostrov's model. The rate of growth is affected by a *directivity*

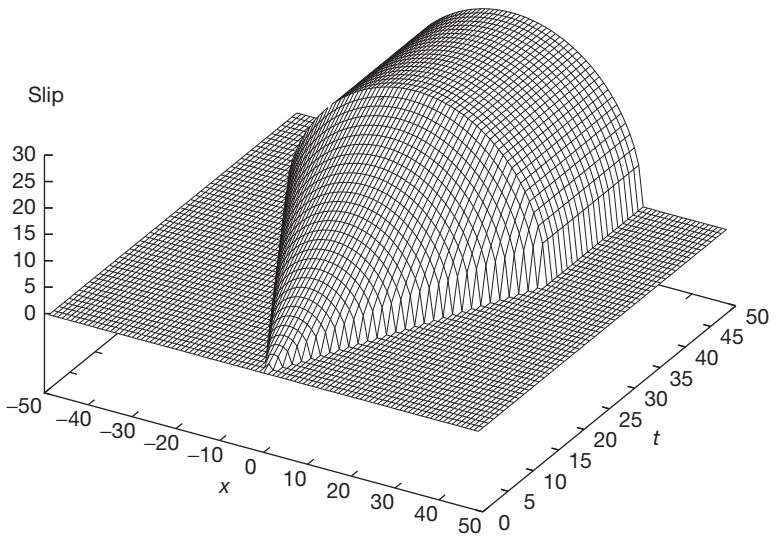

Figure 5 Slip distribution as a function of time on Sato and Hirasawa (1973) circular dislocation model.

factor in the denominator $(1-v_r^2/c^2\sin\theta)^2$ that increases with the polar angle θ and is maximum for $\theta=\pi/2$.

4.02.4.2.2 The kinematic circular source model of Sato and Hirasawa

Simple Kostrov's self-similar crack is not a good seismic source model for two reasons: (1) rupture never stops so that the seismic waves emitted by this source increase like t^2 without limit and (2) it does not explain the high-frequency radiation from seismic sources. Sato and Hirasawa (1973) proposed a modification of Kostrov's model that retained its initial rupture behavior [59] but added the stopping of rupture. They assumed that the Kostrov-like growth of the fault was suddenly stopped across the fault when rupture reached a final radius a (see Figure 5). In mathematical terms, the slip function is

$$\begin{aligned}\Delta u_x(r,t) &= C(v_r)\frac{\Delta\sigma}{\mu}\sqrt{v_r^2t^2-r^2}\,\mathrm{H}(v_rt-r) \quad \text{for} \quad t<a/v_r \\ &= C(v_r)\frac{\Delta\sigma}{\mu}\sqrt{a^2-r^2}\,\mathrm{H}(a-r) \quad \text{for} \quad t>a/v_r\end{aligned} \qquad [52]$$

Thus, at $t=a/v_r$, the slip on the fault becomes frozen and no motion occurs thereafter. This mode of healing is noncausal, but the solution is mechanically acceptable because slip near the borders of the fault always tapers like a square root of the distance to the fault tip. Using the far-field radiation approximation [45], Sato and Hirasawa found that the source time function for this model could be computed exactly

$$\Omega_{SH}(t,\theta) = C(v_r)\frac{2\pi}{\left(1-v_r^2/c^2\sin^2\theta\right)^2}\Delta\sigma v_r^3t^2 \qquad [53]$$

for $t<L/v_r(1-v_r/c\sin\theta)$ where θ is the polar angle of the observer. As should have been expected, the initial rise of the radiated field is the same as in Kostrov's model, the initial phase of the source time function increases very fast like t^2. After the rupture stops, the radiated field is

$$\Omega_{SH}(t,\theta) = C(v_r)\frac{\pi}{2}\frac{1}{v_r/c\sin\theta}\left[1-\frac{v_r^2t^2}{a^2(1+v_r/c\sin\theta)^2}\right]\Delta\sigma a^2v_r \qquad [54]$$

for times between $t_{s1}=a/v_r(1-v_r/c\sin\theta)$ and $t_{s2}=a/v_r(1+v_r/c\sin\theta)$. Radiation from the stopping process is spread in the time interval between the two stopping phases emitted from the closest (t_{s1}) and the farthest (t_{s2}) points of the fault. For times greater than t_{s2}, Ω returns to zero. The waves radiated by circular crack present both *directivity* in the second term and strong *focusing* due to the inverse sin θ term. Because of this term, the radiated field Ω is infinite along the axis of the fault.

It is also possible to compute the spectrum of the far-field signal ([53] and [54]) analytically. This was done by Sato and Hirasawa (1973). The important feature of the spectrum is that it is dominated by the stopping phases at times t_{s1} and t_{s2}. The stopping phases are both associated with a slope discontinuity of the source time function. As we already discussed for Brune's model, slope discontinuities produce ω^{-2} high-frequency asymptotes. This simple model explains one of the most universal features of seismic sources: The high frequencies radiated by seismic sources are dominated by stopping phases not by the energy radiated from the initiation of seismic rupture (Savage, 1966). These stopping phases are ubiquitous in dynamic models of faulting.

4.02.4.3 Generalization of Kinematic Models and the Isochrone Method

A simple yet powerful method for understanding the general properties of seismic radiation from classical dislocation models was proposed by Bernard and Madariaga (1984) and Spudich and Frazer (1984). The method was recently extended to study radiation from supershear ruptures by Bernard and Baumont (2005). The idea is that since most of the energy radiated from the fault comes from the rupture front, it should be possible to find where energy is coming from at a given station and at a given time. Bernard and Madariaga (1984) originally derived the isochrone method by inserting the ray-theoretical expression [22] into the representation theorem, a technique that is applicable not only in the far field but also in the immediate vicinity of the fault at high frequencies. Here, for the purpose of simplicity, we derive isochrones only in the far field. For that purpose, we study the far-field source time function for a finite fault derived in [45]. We assume that the slip rate distribution has the general form

$$\Delta\dot{u}_i(\xi_1,\xi_2,t) = D_i(t-\tau(\xi_1,\xi_2)) = D_i(t)*\delta(t-\tau(\xi_1,\xi_2)) \qquad [55]$$

where $\tau(\xi_1,\xi_2)$ is the rupture delay time at a point of coordinates ξ_1,ξ_2 on the fault. This is the time that it takes for rupture to arrive at that point. The star indicates time-domain convolution. We rewrote [55] as a convolution in order to distinguish between the slip time function $D(t)$ and its propagation along the fault described by the argument to the delta function. While we assume here that $D(t)$ is strictly the same everywhere on the fault, in the spirit of ray theory, our result remains valid if $D(\xi_1,\xi_2,t)$ is a slowly variable function of position on the fault. Inserting the slip rate field [55] in the source time function [45], we get

$$\Omega(t,\theta,\phi) = \mu D_i(t)*\int_0^t\int_{S_0}\delta\left[t-\tau(\xi_1,\xi_2)-\frac{\mathbf{e}\cdot\mathbf{x}_0}{c}\right]\mathrm{d}^2\mathbf{x}_0\mathrm{d}\tau \qquad [56]$$

where the star indicates time-domain convolution. Using the sifting property of the delta function, the integral over the fault surface S_0 reduces to an integral over a line defined implicitly by

$$t = \tau(\xi_1,\xi_2)+\frac{\mathbf{e}\cdot\mathbf{x}_0}{c} \qquad [57]$$

the solutions of this equation define one or more curves on the fault surface (see Figure 6). For every value of time, eqn [57] defines a curve on the fault that we call an isochrone.

The integral over the surface in [56] can now be reduced to an integral over the isochrone using standard properties of the delta function

$$\Omega(t,\theta,\phi) = \mu D_i(t)*\int_{l(t)}\frac{\mathrm{d}t}{\mathrm{d}n}\mathrm{d}l \qquad [58]$$

$$= \mu D_i\pi(t)*\int_{l(t)}\frac{v_r}{(1-v_r/c\cos\psi)}\mathrm{d}l \qquad [59]$$

where $l(t)$ is the isochrone and $\mathrm{d}t/\mathrm{d}n=\mathbf{n}\cdot\nabla_{x_0}t=v_r/(1-v_r/c\cos\psi)$ is the derivative of t in the direction perpendicular to the

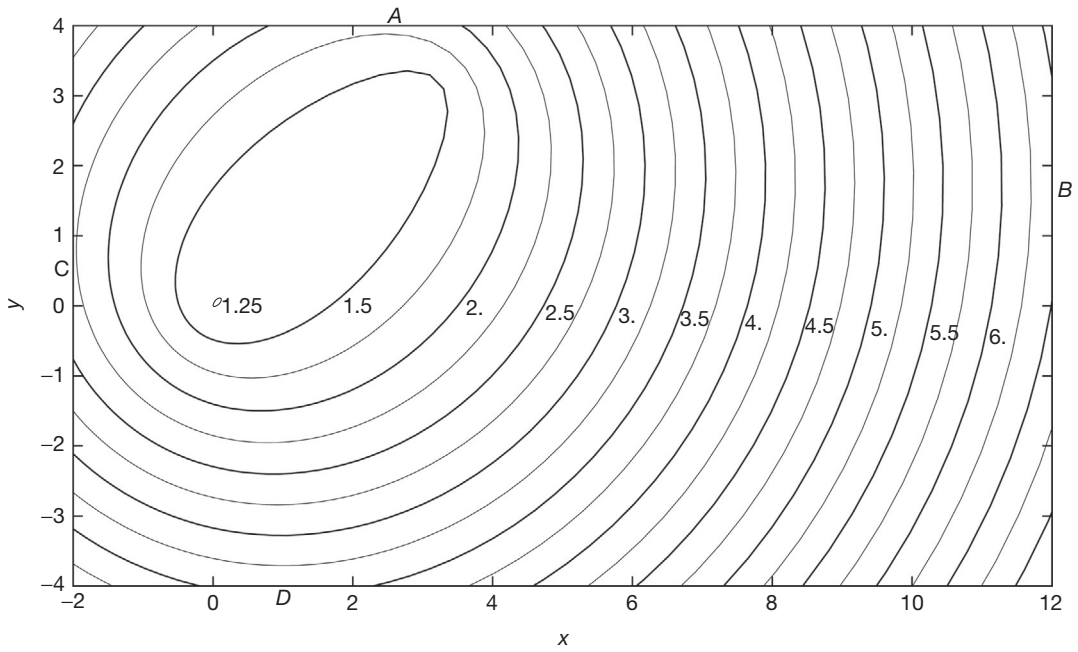

Figure 6 Example of an isochrone. The isochrone was computed for an observer situated at a point of coordinates (3.,3.,1.) in a coordinate system with origin at the rupture initiation point (0.,0.). The vertical axis is out of the fault plane. Rupture starts at $t=0$ at the origin and propagates outward at a speed of 90% the shear wave speed that is 3.5 km s^{-1} in this computation. The signal from the origin arrives at $t=1.25$ s at the observation point. Points A–D denote the location on the border of the fault where isochrones break, producing strong stopping phases.

isochrone. Actually, as shown by Bernard and Madariaga (1984), dt/dn is the local directivity of the radiation from the isochrone. In general, both the isochrone and the normal derivative dt/dn have to be evaluated numerically. The meaning of [58] is simple, the source time function at any instant of time is an integral of the directivity over the isochrone.

The isochrone summation method has been presented in the simplest case here, using the far-field approximation. The method can be used to compute synthetics in the near field too; in that case, changes in the radiation pattern and distance from the source and observer may be included in the computation of the integral [58] without any trouble. The results are excellent as shown by Bernard and Madariaga (1984) who computed synthetic seismograms for a buried circular fault in a half-space and compared them to full numerical synthetics computed by Bouchon (1982). With improvements in computer speed, the use of isochrones to compute synthetics is less attractive, and although the method can be extended to complex media within the ray approximation, most modern computations of synthetics require the appropriate modeling of multipathing, channeled waves, etc. that are difficult to integrate into the isochrone method. Isochrones are still very useful to understand many features of the radiated field and its connection to the rupture process (see, e.g., Bernard and Baumont, 2005).

4.02.5 Crack Models of Seismic Sources

As we have mentioned several times, dislocation models capture some of the most basic geometric properties of seismic sources but have several unphysical features that require careful consideration. For small earthquakes, the kinematic models are generally sufficient, while for larger events – especially in the near field – dislocation models are inadequate because they may not be used to predict high-frequency radiation. A better model of seismic rupture is of course a crack model like Kostrov's self-similar crack. In crack models, slip and stresses are related in a very precise way, so that a finite amount of energy is stored in the vicinity of the crack. Griffith (1920) introduced crack theory using the only requirement that the appearance of a crack in a body does two things: (1) it relaxes stresses and (2) it releases a finite amount of energy. This simple requirement is enough to define many of the properties of cracks, in particular energy balance (see, e.g., Freund, 1989; Kostrov and Das, 1988; Rice, 1980; see also **Chapter 4.03**, Fracture and Frictional Mechanics).

Let us consider the main features of a crack model. Referring to **Figure 7**, we consider a planar fault lying on the plane x, y with normal z. Although the rupture front may have any shape, it is simpler to consider a linear rupture front perpendicular to the x-axis and moving at speed v_r in the positive x direction. Three modes of fracture can be defined with respect to the configuration of **Figure 7**:

- Antiplane, mode III or SH, when slip is in the y direction and stress drops also in this direction, that is, stress σ_{zy} is relaxed by slip.
- Plane, or mode II, when slip is in the x direction and stress drops also in this direction, that is, stress σ_{zx} is relaxed by this mode.
- Opening, or mode I, when the fault opens with a displacement discontinuity in the z direction. In this case, stress σ_{zz} drops to zero.

In natural earthquakes, the opening mode is unlikely to occur at large scales, although it is perfectly possible for very

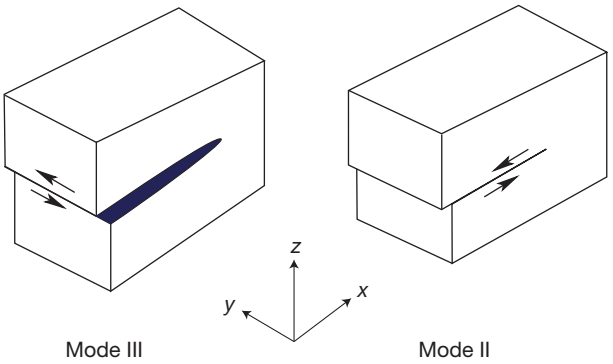

Figure 7 Modes of rupture for shear faulting. Mode III or antiplane mode and mode II or inplane mode may occur at different places on fault boundaries. For general faulting models, both modes occur simultaneously.

small cracks to appear due to stress concentrations, geometric discontinuities of the fault, etc.

For real ruptures, when the rupture front is a curve (or several disjoint ruptures if the source is complex), modes II and III will occur simultaneously on the periphery of the crack. This occurs even in the simple self-similar circular crack model we studied earlier. Fortunately, in homogeneous media, except near-sharp corners and strong discontinuities, the two modes are locally uncoupled, so that most features determined in 2-D carry over to 3-D cracks with little change.

In order to study a two-dimensional crack model, we solve the elastodynamic wave equation together with the following boundary conditions on the $z=0$ plane. For antiplane cracks, mode III:

$$\begin{aligned} \sigma_{zy}(x,0) &= \Delta\sigma \quad \text{for} \quad x < l(t) \\ u_y(x,0) &= 0 \quad \text{for} \quad x > l(t) \end{aligned} \qquad [60]$$

For plane cracks, mode II:

$$\begin{aligned} \sigma_{zx}(x,0) &= \Delta\sigma \quad \text{for} \quad x < l(t) \\ u_x(x,0) &= 0 \quad \text{for} \quad x > l(t) \end{aligned} \qquad [61]$$

where $l(t)=v_r t$ is the current position of the rupture front on the x-axis. These boundary conditions define a mixed boundary value problem that can be solved using complex variable techniques. The solution for arbitrary time variation of $l(t)$ was found for mode III by Kostrov (1966). For plane ruptures, the solution for arbitrary $l(t)$ was found by Freund (1972) (see also Kostrov and Das, 1988). Eshelby (1969) showed that the crack problems have a number of universal features, which are independent of the history of crack propagation and depend only on the instantaneous rupture speed.

4.02.2.5.1 Rupture Front Mechanics

Since stresses and velocities around a rupture front have universal properties, we can determine them by studying the simpler crack that propagates indefinitely at constant speed. This can be done using a Lorentz transformation of the static elasticity. We are not going to enter in the details of the determination of the solution of the wave equation in moving coordinates; very succinctly, the stress and velocity fields

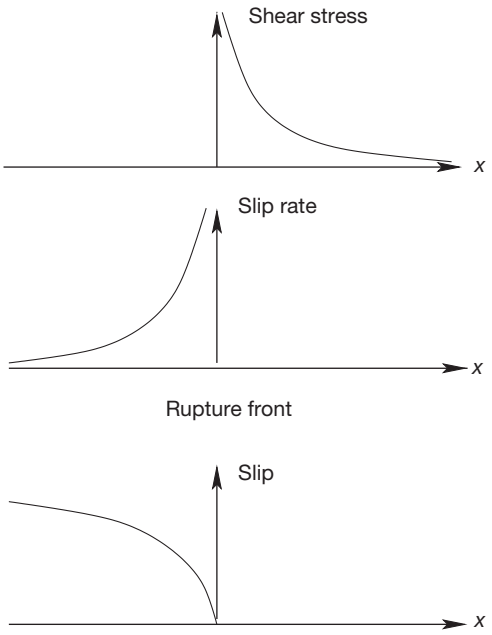

Figure 8 State of stress and slip velocity near the tip of a fracture propagating with a rupture speed less than that of Rayleigh waves.

around the crack tip are related by a nonlinear eigenvalue problem solved by Muskhelishvili in his classical work on complex potentials. There are an infinite number of solutions of the problem, but only one of them ensures a finite energy flow into the crack tip. All other produce no flow or infinite flow.

Along the fault, stress and particle velocities have the universal forms (see Figure 8)

$$\begin{aligned} \sigma(x) &= \frac{K}{\sqrt{2\pi}} \frac{1}{[x-l(t)]^{1/2}} \quad \text{for} \quad x > l(t) \\ \Delta\dot{u}(x) &= \frac{V}{\sqrt{2\pi}} \frac{1}{[x-l(t)]^{1/2}} \quad \text{for} \quad x < l(t) \end{aligned} \qquad [62]$$

and the relations [60] or [61] on the rest of the line. Here, σ stands for either σ_{yz} or σ_{xz} and $\Delta\dot{u}$ for the corresponding slip velocity component in either antiplane or plane fracture modes. In [62], K is the stress concentration, a quantity with units of Pa $m^{1/2}$ that represents the strength of the stress field near the rupture front. V is the dynamic slip rate intensity, which is related to K by

$$K = \frac{\mu}{2v_r}\sqrt{1-v_r^2/\beta^2}\,V \qquad [63]$$

for antiplane cracks, where μ and β are the elastic rigidity and shear wave speed, respectively. For plane cracks, the relation is more complicated

$$K = \frac{\mu}{2v_r}\frac{\beta^2}{v_r^2}\frac{R(v_r)}{\sqrt{1-v_r^2/\beta^2}} \qquad [64]$$

where $R(v_r)$ is the Rayleigh function

$$R(v_r) = 4\sqrt{1-v_r^2/\beta^2}\sqrt{1-v_r^2/\alpha^2} - \left(2-v_r^2/\beta^2\right)^2$$

The complete angular dependence of the stress and particle velocity fields is given by Freund (1989). The inverse squared-root singularities of the form [62] only occur if the rupture velocity is less than the classical limiting rupture speeds: the shear wave velocity β for antiplane ruptures and the Rayleigh wave speed $c_R \approx 0.91\beta$ for inplane cracks. At the terminal speed, the coefficient relating K and V reduces to zero, meaning that at the terminal speed the stress concentration K disappears. A crack running at the terminal speed releases no energy; this speed is thus only possible if there are no rupture resistance and no friction on the fault.

Both experimental evidence and observational evidence cited by Rosakis et al (1999) showed that it is possible for mode II shear cracks to propagate at speeds faster than the shear wave speed in a so-called supershear mode first put in evidence numerically by Andrews (1976). For supershear speeds, the stress and velocity concentration have different dependence with distance than the squared root for subshear faults except for a very particular rupture speed $\sqrt{2}\beta$, sometimes called the Eshelby speed.

The stress field in [62] is infinite at the rupture front; this is a consequence of the idealization that was made to obtain these results: It was assumed that the material around the fault remained elastic even in the immediate vicinity of the rupture front. If more realistic frictional boundary conditions are used instead of the abrupt discontinuities implied by [60] and [61], then the singularity disappears inside a small zone called the rupture process, or slip-weakening zone. Many global features of the crack model can be derived with the simple elastic model studied here; more detailed studies involving a finite slip-weakening zone are only needed to study crack growth in detail.

4.02.5.2 Stress and Velocity Intensity

K and V in [62] have a simpler more fundamental structure that was discovered by Eshelby (1969) for the antiplane case and later extended to plane shear cracks by many authors as reviewed by Freund (1989). Both the dynamic stress intensity factor and the velocity intensity factors can be written in the form

$$\begin{aligned} K &= k(v_r)K^* \\ V &= b(v_r)V^* \end{aligned} \qquad [65]$$

where, for an antiplane crack,

$$k_{III}(v_r) = \sqrt{1 - v_r/\beta}$$

and, for a mode II crack,

$$k_{II}(v_r) \approx 1 - v_r/c_r$$

which is a very good approximation; the exact expression for k_{II} can be found in the books by Freund (1989) and Kostrov and Das (1988).

The factors K^* and V^* in [65] depend only on the load applied to the fault. In the case of an earthquake, they are determined by the stress drop inside those segments of the fault that have already slipped. Since $k(v_r) \to 0$ as the rupture velocity tends to zero, K^* is simply the stress intensity that would prevail if the rupture velocity dropped instantaneously to zero. Thus, K^* is often called the zero-speed stress intensity factor; it depends only on the history of rupture and stress drop inside the broken parts of the fault. Some authors interpret this property of faults mechanics as meaning that rupture fronts have no inertia and their rupture speed can change instantaneously if rupture resistance increases or if the rupture front encounters some geometric discontinuity like a fault jog or a kink.

4.02.5.3 Energy Flow into the Rupture Front

We already mentioned that the stress and slip singularities are a consequence of the requirement that there is a finite energy flow into the rupture front. This energy is used to create new fault surface and is spent in overcoming frictional resistance of the fault. The energy flow into the crack tip was first computed by Kostrov and Nikitin (1970) who provided a very complete discussion of the problem.

The energy flow per unit area of crack advance is usually called G_c

$$G_c = \frac{1}{4v_r} KV \qquad [66]$$

for all the modes, so that for mode III,

$$G_{III} = \frac{1}{2\mu} \frac{1}{\sqrt{1 - v_r^2/\beta^2}} K^2$$

and, for mode II,

$$G_{II} = \frac{1}{2\mu} \frac{v_r^2}{\beta^2} \frac{\sqrt{1 - v_r^2/\beta^2}}{R(v_r)} K^2$$

Let us note that K^2 tends to zero as the rupture velocity v_r approaches the Rayleigh wave speed, so that G_{II} vanishes at the terminal speed.

The crack models are mostly concerned with the local conditions near the edge of the fault as it propagates inside the elastic medium. This is the principal subject of fracture mechanics. In seismology, we are interested not only on the growth of ruptures but also on the generation of seismic waves. Earthquakes are three-dimensional and the finiteness of the source plays a fundamental role in the generation of seismic waves.

4.02.5.4 The Circular Crack

The simplest fault model that can be imagined is a simple circular crack that grows from a point at a constant or variable rupture speed and then stops on the rim of the fault arrested by the presence of unbreakable barriers. The first such simple model was proposed by Madariaga (1976). Although this model is unlikely to represent any actual earthquake, it does quite a good job in explaining many features that are an intrinsic part of seismic sources, most notably the scaling of different measurable quantities, like slip, slip rate, stress change, and energy release. The circular crack problem is posed as a crack problem, which is in terms of stresses not of slip.

We start by a quick study of a simple circular crack from which we derive some of the most fundamental properties of dynamic source models. Let us consider a static circular ('penny-shaped') crack of radius a lying on the x, y plane. Assuming that the fault is loaded by an initial shear stress σ^0_{xz} and that the stress drop

$$\Delta\sigma = \sigma^0_{xz} - \sigma^f_{xz}$$

is uniform, where σ^f_{xz} is the final, residual stress in the fault zone (Chapters 4.08 and 4.06), the slip on the fault is given by

$$\Delta u_x(r) = D(r) = \frac{24}{7\pi}\frac{\Delta\sigma}{\mu}\sqrt{a^2 - r^2} \qquad [67]$$

where r is the radial distance from the center of the crack on the (x, y) plane, a is the radius of the crack, and μ is the elastic rigidity of the medium surrounding the crack (see Figure 9). Slip in this model has the typical elliptical shape that we associate with cracks and is very different from the constant slip inside the fault assumed in Haskell's model. The taper of the slip near the edges of the crack is of course in agreement with what we discussed about the properties of the elastic fields near the edge of the fault. From [67], we can determine the scalar seismic moment for this circular fault

$$M_0 = \frac{16}{7}\Delta\sigma a^3 \qquad [68]$$

so that the moment is the product of the stress drop times the cube of the fault size. This simple relation is the basis of the seismic scaling law proposed by Aki (1967). The circular crack model has been used to quantify numerous small earthquakes for which the moment was estimated from the amplitude of seismic waves and the source radius was estimated from corner frequencies, aftershock distribution, etc.; the result is that for shallow earthquakes in crustal seismogenic zones like the San Andreas Fault or the North Anatolian Fault in Turkey, stress drops are of the order of 1–10 MPa. For deeper events in subduction zones, stress drops can reach several tens of MPa. Thus, in earthquakes, stresses do not change much, at most a couple of order of magnitudes, while source radius varies over several orders of magnitudes from meters to 100 km or more. It is only in this sense that the usual assertion 'stress drop in earthquakes is constant' should be taken; it actually changes but much less than the other parameters in the scaling law.

Finally, let us take a brief view of the stress field in the vicinity of the fault radius. As expected for crack models, the stress presents stress concentrations of the type [62], that is,

$$\sigma_{xz}(r, \phi) = \frac{(K_{II}\cos\phi + K_{III}\sin\phi)}{\sqrt{r - a}}$$

where (r, ϕ) are polar coordinates on the plane of the circular fault with ϕ being measured from the x-axis. The stress intensity factors are

$$K_{II} = \frac{16}{7\sqrt{\pi}}\frac{1}{1-\nu}\Delta\sigma\sqrt{a} \quad \text{and} \quad K_{III} = \frac{16}{7\sqrt{\pi}}\Delta\sigma\sqrt{a}$$

where ν is Poisson's ratio. It is interesting to note that even if the slip distribution [67] was radially symmetrical, the stress distribution is not. Stress concentration in the mode II direction is stronger than in the antiplane one. As a consequence, if rupture resistance is the same in plane and antiplane modes, a circular crack has an unstable shape. This is clearly observed in fully dynamic simulations where the faults become invariably elongated in the inplane direction.

The creation of a static circular crack with slip [67] inside an elastic medium of rigidity μ produces an elastic energy release

$$\Delta U = \frac{8}{7}\frac{\Delta\sigma^2}{\mu}a^3 \qquad [69]$$

This is the maximum energy that is available for radiation from the dynamic rupture of the circular crack. In reality, the creation of the crack reduces the amount of energy radiated by the energy required to generate the new fault surface.

The simplest physically realistic source model is a circular crack that grows initially at constant speed v_r as predicted by the self-similar Kostrov's model [51] for times less than a/v_r and then evolves spontaneously while it heals. Such a model is usually called quasidynamic because rupture speed is imposed but slip is computed from a properly posed mechanical problem (Madariaga, 1976). There are no simple analytic solutions equivalent to that of Sato and Hirasawa (1973) for quasidynamic cracks. We are forced to use numerical solutions that are actually very simple to obtain using either finite difference or boundary integral equation techniques. The full solution to the circular crack problem is shown in Figure 10. Initially, until the sudden arrest of rupture at the final radius a, the slip distribution can be accurately computed using Kostrov's self-similar solution [51]. The stopping of rupture generates strong healing waves that propagate inward from the rim of the fault. These waves are of three types: P-, S-, and Rayleigh waves. Soon after the passage of the Rayleigh waves, slip rate inside the fault decreases to zero and the fault heals. After healing, we assume that frictional forces are sufficiently strong that no slip will

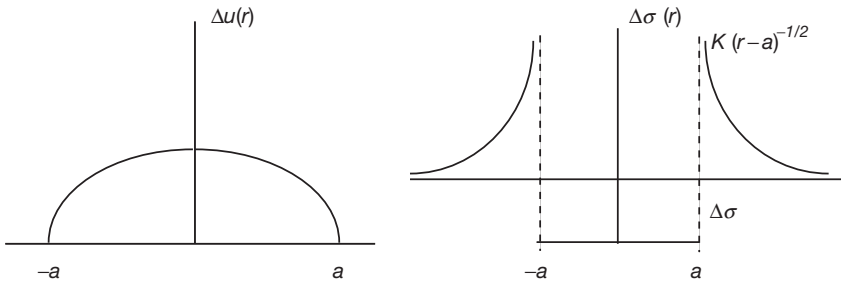

Figure 9 Static circular crack model. On the left, the slip distribution as a function of radius of the fault. On the right, the corresponding shear stress change. Inside the fault, stress drops by a constant amount, and outside the fault, inverse square root stress concentrations appear.

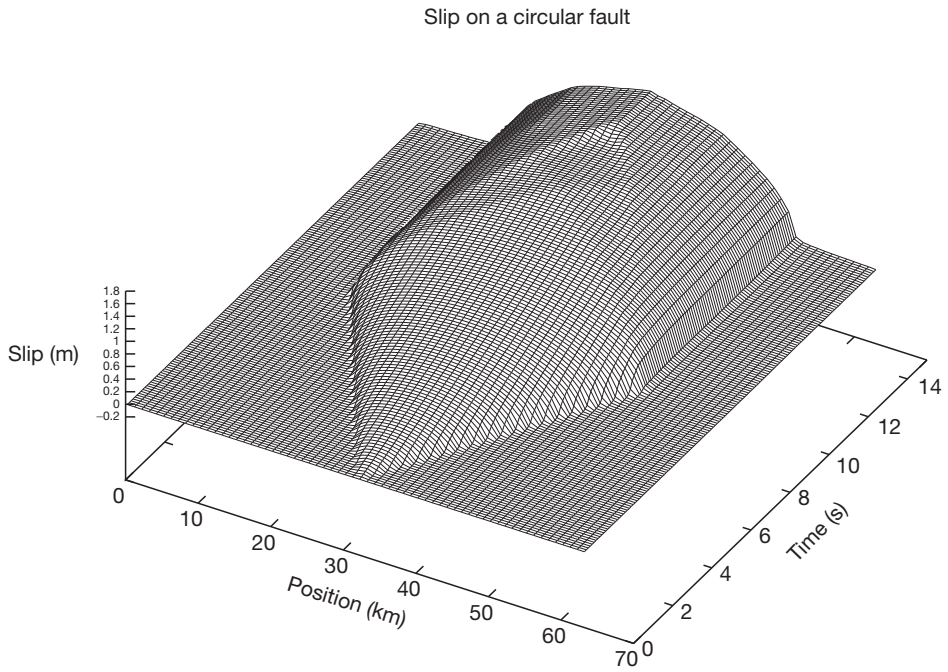

Figure 10 Slip distribution as a function of time and position for a quasidynamic circular crack model. The healing phases, emitted by the border of the fault, are clearly observed. These are the P-, S-, and Rayleigh waves emitted by the circular border of the fault when rupture suddenly arrests.

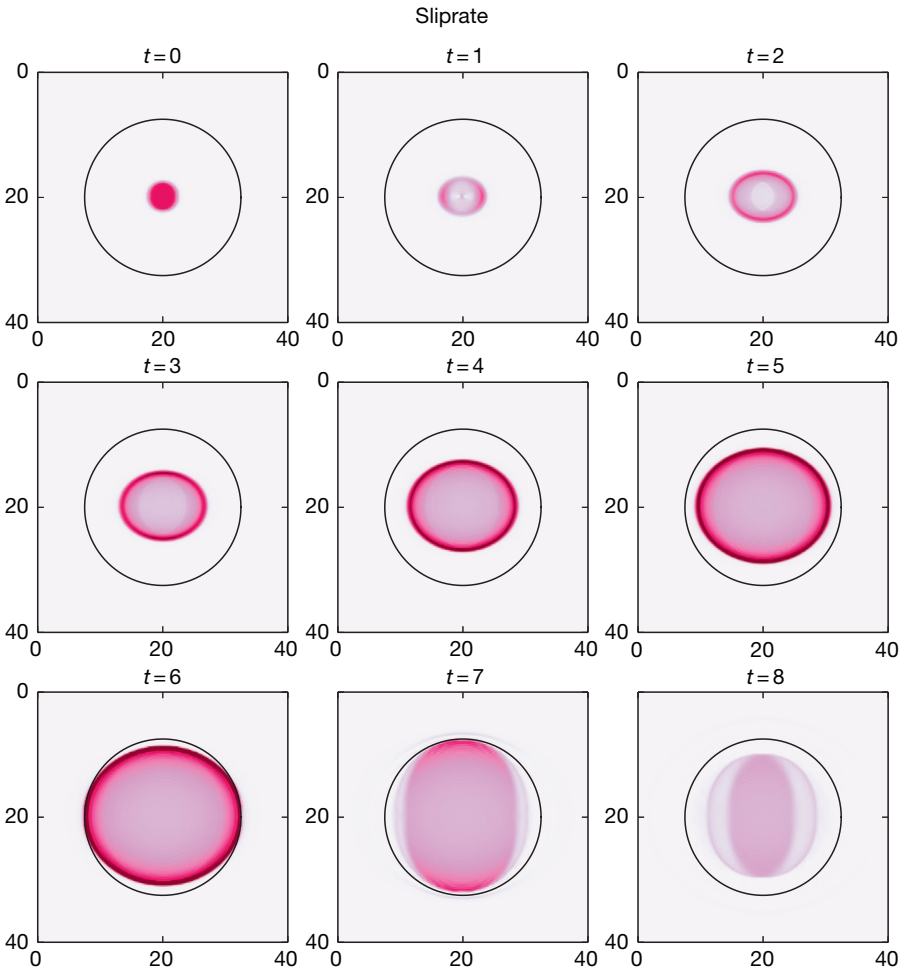

Figure 11 Slip rate on a dynamic circular shear fault. Rupture propagates spontaneously until it reaches an unbreakable circular barrier shown by the black circle. The snapshots depict the slip rate inside the fault at successive instants of time. The darker colors indicate larger values of slip rate, with a scaling ranging from 0 to 1.27 m s^{-1}.

occur until the fault is reloaded. As observed in Figure 10, it is clear that slip and rise time are functions of position on the fault, the rise time being much longer near the center where slip is also larger than near the edges of the fault where slip is clamped. Finally, let us note that the slip after healing is very similar to that of a static circular crack, except that there is an overshoot of slip with respect to the static solution [67]. The overshoot is of course a function of the rupture speed, but its maximum value is of the order of 15% for a rupture speed of 0.75β. The quasidynamic circular crack model was recently studied with a high-resolution numerical method by Kaneko and Shearer (2014). Their results are similar to those of Madariaga (1976) except that the numerical coefficient relating the corner frequency to the radius of the fault has increased. We refer to them for a detailed study of the radiation from the circular crack. Here, we turn to fully dynamic sources.

4.02.5.5 The Dynamic Circular Fault in a Homogenous Medium

The circular crack model was originally proposed by Brune (1970) to explain the omega-squared model of the radiated spectrum. This model is widely used to obtain information about seismic sources, to compute stress change and radiated energy. In this section, we study the spontaneous propagation of rupture away from a small initial asperity that is arrested by an unbreakable circular barrier. This is the simplest realistic source model that we can study. Our study will show the role of rupture propagation, stopping phases, and healing phases for a very simple geometry.

We modeled a circular fault embedded inside a homogeneous elastic medium where P-wave velocity was 6400 m s^{-1}, the P-to-S velocity ratio was 1.73, and the density was 2700 Kg m^{-3}. Stress drop, the difference between initial stress in the fault and the residual stress after slip rate has decreased to zero, was 4.5 MPa. In the dynamic model, rupture propagation is controlled by a slip-weakening friction law (Ida, 1972) with a peak stress of 8 MPa, a slip-weakening distance of 0.2 m, and an energy release rate of $G_c = 0.8$ J m^{-2} (Chapter 4.06).

We modeled the circular fault using a staggered grid finite difference code proposed by Madariaga et al (1998). The space and time steps were 200 m and 0.01 s, respectively. Rupture starts from a small circular asperity where stress is at the static friction level and then propagates spontaneously until it is arrested by an unbreakable barrier of radius of 20 km concentric with the initial asperity. Since we are interested in comparing spontaneous rupture simulations with the quasidynamic circular crack model, we used a stress drop of 4.5 MPa so that the rupture does not become supershear in our simulation. Snapshots of slip rate are shown in Figure 11 at several successive instants of time measured in seconds. We observe that after 2 s, rupture has become elongated in the horizontal direction, which is also the direction of the initial stress. In this direction, mode II prevails. In the transverse direction (vertical), slip is in mode III. Thus, as already remarked by Das (1980) and Day (1982), rupture tends to grow faster in the inplane direction, which is dominated by mode II. At time $t = 6$ s, rupture has reached the unbreakable border of the fault in the inplane direction, and at time $t = 7$ s, the stopping phases generated by the top and bottom edges of the fault have started to move toward the center of the fault. The snapshot at $t = 8$ s shows stopping phases propagating inward from all directions. The slipping patch in darker color is now elongated in the antiplane direction, which is due to slower healing. The duration of the rupture process is slightly longer than 8 s.

Let us now study the radiation from the dynamic circular fault. These circular crack models are widely used to study seismic radiation. How much does *spontaneous rupture* affect the radiation of circular crack models? As expected for a finite rupture model, there are significant variations in the seismic signals radiated in different direction of space. To illustrate this variability, we show in Figure 12 the radiation in two directions: along the mode II direction and along the transverse or mode III direction. The angle θ is the polar angle measured from the normal to the fault plane, and ϕ is the azimuth measured from the direction of slip on the fault. The displacement signals are shown in Figure 12 in two different directions ($\phi = 0°$ and $\phi = 90°$). Both have roughly the same duration of about 10 s but are quite different because one of them ($\phi = 90°$) has larger displacement at the beginning of the signal, while the other is stronger near the end. The reason is that stopping phases, the abrupt change in slope in the figures,

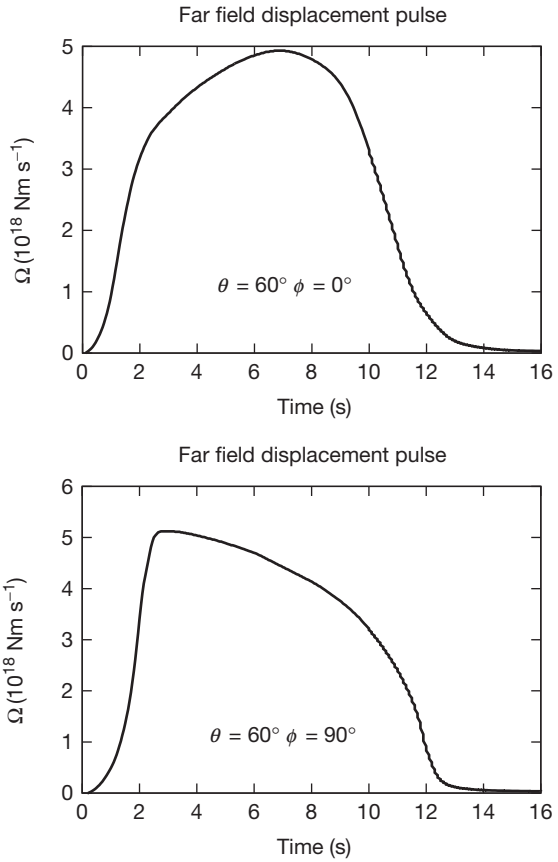

Figure 12 Far-field pulses radiated by the circular crack in two directions of space: θ is the polar angle measured from the axis of the circular crack and ϕ is the azimuth measured from the direction of slip. Thus, $\phi = 0$ is the direction of inplane motion (mode II) and $\phi = 90°$ is the direction of mode III.

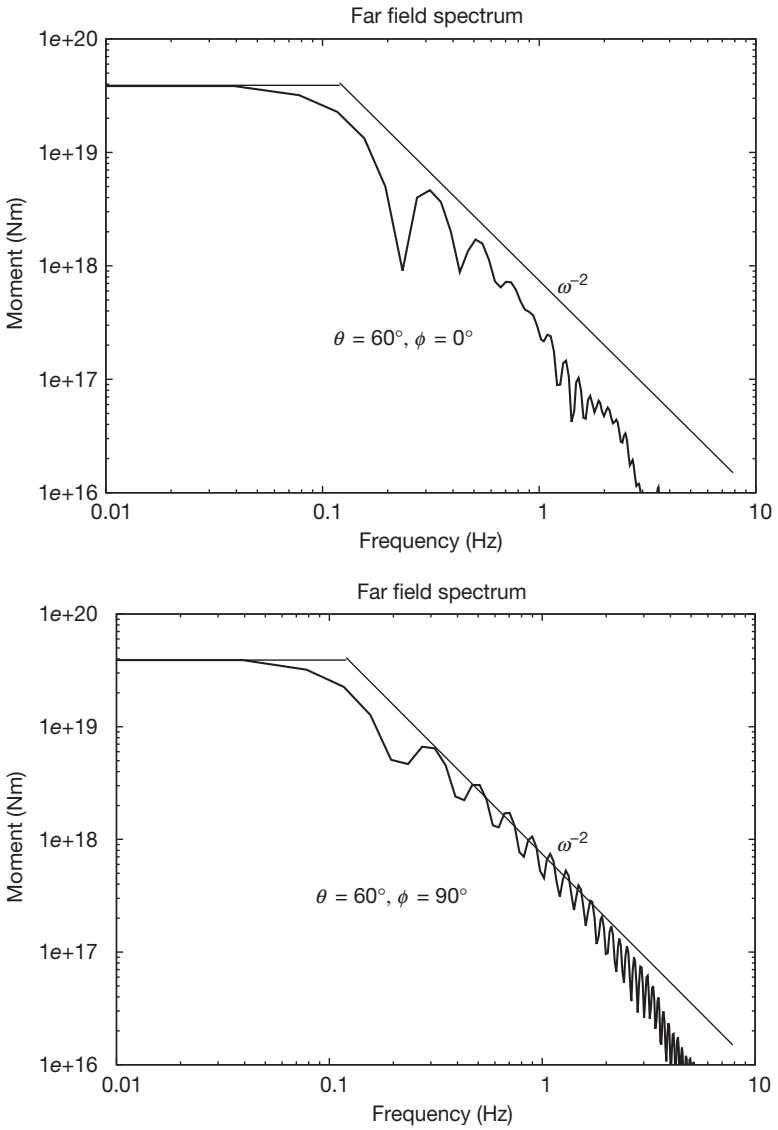

Figure 13 Far-field Fourier spectrum for the two far-field signals shown in **Figure 12**. The spectra have the typical inverse ω-squared decay at high frequencies.

have different relative weights. This difference is in turn due to directivity that is very large in the forward direction ($\phi = 0°$) and is minimal in the transverse direction ($\phi = 90°$). The corresponding amplitude spectra are shown in **Figure 13**. As predicted by Aki (1967) and Brune (1970), these have the typical ω^{-2} spectral decay at high frequencies. The corner frequencies vary from 0.1 to 0.12 Hz. It is not surprising that very different time-domain signals produce similar spectra. The reason is that spectra are dominated by the stopping phases, which carry the information about *rupture arrest*. Although arrest is faster in the inplane direction, the difference in arrival time of the stopping phases is not very large so that the main features of the spectrum are preserved. It is possible to study the variation of corner frequency as a function of the polar angle and azimuth, but the effect of moving the initiation point with respect to the circular border is much more important.

4.02.6 Conclusions

The study of seismic radiation from realistic source models has reached now its maturity. Seismologists have been able to invert the rupture process of a number of earthquakes, and many of the features predicted by simple dynamic source models have been quantified and observed. Foremost among these is the shape of the far-field spectrum, the basic scaling laws relating particle velocity and acceleration to properties of the fault, like size, stress drop, and rupture velocity. The frontier today is the accurate estimation and interpretation of seismic energy and, therefore, the quantification of radiation in terms of the energy balance of seismic sources.

Recent inversions of earthquake slip distributions using kinematic source models have found very complex source

distributions that require an extensive reappraisal of classical source models that were mostly based on Kostrov's model of self-similar circular crack. Ruptures in a fault with heterogeneous stress and rupture resistance distributions follow very tortuous paths. While on the average, the rupture propagates at a sub-Rayleigh speed from one end of the fault to another, in detail, the rupture front can wander in all directions following the areas of strong stress concentration and avoiding those with low stress or high rupture resistance. If this view of earthquake rupture was to be confirmed by future observations (we believe it will be), then many current arguments about earthquake complexity, narrow rupture pulses, and earthquake distributions will be solved, and we may concentrate on the truly interesting problem of determining which features of friction determine that fault stress is always complex under all circumstances.

Acknowledgments

I am greatly indebted to Drs. Shamita Das and John Boatwright for their enlightening comments about the initial version of this manuscript. This research was supported by ANR (Agence nationale de la recherche) under contract S4 ANR-11-BS56-0017.

References

Achenbach JD (1975) *Wave Propagation in Elastic Solids*. Amsterdam: North Holland.

Aki K (1966) Generation and propagation of G waves from the Niigata earthquake of June 16, 1964. Estimation of earthquake movement, released energy and stress-strain drop from G-wave spectrum. *Bulletin of the Earthquake Research Institute* 44: 73–88.

Aki K (1967) Scaling law of seismic spectrum. *Journal of Geophysical Research* 73: 5359–5376.

Aki K and Richards PG (2002) *Quantitative seismology*, 2nd edn. Sausalito, California: University Science Books.

Ampuero J-P and Dahlen FA (2005) Ambiguity of the Moment Tensor. *Bulletin of the Seismological Society of America* 95: 390–400.

Andrews J (1976) Rupture velocity of plane strain shear cracks. *Journal of Geophysical Research* 81: 5679–5687.

Backus G and Mulcahy M (1976) Moment tensors and other phenomenological descriptions of seismic sources. I Continuous displacements. *Geophysical Journal of the Royal Astronomical Society* 46: 321–361.

Ben Menahem A (1961) Radiation of seismic surface waves from finite moving sources. *Bulletin of the Seismological Society of America* 51: 401–435.

Ben Menahem A (1962) Radiation of seismic body waves from finite moving sources. *Journal of Geophysical Research* 67: 345–350.

Ben Menahem A and Singh SJ (1981) *Seismic Waves and Sources*. New York: Springer.

Bernard P and Baumont D (2005) Shear Mach wave characterization for kinematic fault rupture models with constant supershear rupture velocity. *Geophysical Journal International* 162: 431–447.

Bernard P and Madariaga R (1984) A new asymptotic method for the modeling of near-field accelerograms. *Bulletin of the Seismological Society of America* 74: 539–557.

Boatwright J (1980) A spectral theory for circular seismic sources: Simple estimates of source dimension, dynamic stress drop, and radiated seismic energy. *Bulletin of the Seismological Society of America* 70: 1–27.

Bouchon M (1982) The rupture mechanism of the Coyote Lake earthquake of August 6, 1979 inferred from near field data. *Bulletin of the Seismological Society of America* 72: 745–759.

Burridge R and Knopoff L (1964) Body force equivalents for seismic dislocations. *Bulletin of the Seismological Society of America* 54: 1875–1878.

Brune J (1970) Tectonic stress and the spectra of seismic shear waves from earthquakes. *Journal of Geophysical Research* 75: 4997–5009.

Cotton F and Campillo M (1995) Frequency domain inversion of strong motions: Application to the 1992 Landers earthquake. *Journal of Geophysical Research* 100: 3961–3975.

Das S (1980) A numerical method for determination of source time functions for general 3 dimensional rupture propagation. *Geophysical Journal of the Royal Astronomical Society* 62: 591–604.

Dziewonski AM and Woodhouse JH (1983) Studies of the seismic source using normal-mode theory. In: Kanamori H and Boschi E (eds.) *Earthquakes: Observation, Theory, and Interpretation: Notes from the International School of Physics "Enrico Fermi" (1982: Varenna, Italy)*, pp. 45–137. Amsterdam: North-Holland Publication.

Eshelby JD (1956) The continuum theory of lattice defect. In: Seitz F and Turnbull D (eds.) *Progress in Solid State Physics*, vol. 4. New York: Academic Press.

Eshelby JD (1969) The elastic field of a crack extending nonuniformly under general antiplane loading. *Journal of the Mechanics and Physics of Solids* 17: 177–199.

Freund LB (1972) Crack propagation in an elastic solid subjected to general loading. II. Nonuniform rate of extension. *Journal of the Mechanics and Physics of Solids* 20: 141–152.

Freund LB (1989) *Fracture Dynamics*. Cambridge, UK: Cambridge University Press.

Fukuyama E and Madariaga R (1995) Integral equation method for plane crack with arbitrary shape in 3D elastic medium. *Bulletin of the Seismological Society of America* 85: 614–628.

Griffith AA (1920) The phenomenon of rupture and flow in solids. *Philosophical Transactions of the Royal Society (London)* A221: 163–198.

Hanks TC and Kanamori H (1979) Moment magnitude scale. *Journal of Geophysical Research* 84: 2348–2350.

Hartzell SH and Heaton TH (1983) Inversion of strong ground motion and teleseismic waveform data for the fault rupture history of the Imperial Valley, California, earthquake. *Bulletin of the Seismological Society of America* 73: 1553–1583.

Haskell NA (1964) Total energy spectral density of elastic wave radiation from propagating faults. *Bulletin of the Seismological Society of America* 54: 1811–1841.

Haskell NA (1966) Total energy spectral density of elastic wave radiation from propagating faults, Part II. *Bulletin of the Seismological Society of America* 56: 1811–1841.

Hirose S and Achenbach JD (1989) Time-domain boundary element analysis of elastic wave interaction with a crack. *International Journal of Mechanical Engineering* 28: 629–644.

Honda H (1962) Earthquake mechanism and seismic waves. *Journal of Physics of the Earth* 10: 1–98.

Ida Y (1972) Cohesive force across the tip of a longitudinal-shear crack and Griffith's specific surface energy. *Journal of Geophysical Research* 77: 2156–2202.

Kanamori H (1977) The energy release in great earthquakes. *Journal of Geophysical Research* 82: 2921–2987.

Kaneko Y and Shearer P (2014) Seismic source spectra and estimated stress drop derived from cohesive-zone models of circular sub-shear rupture. *Geophysical Journal International*. http://dx.doi.org/10.1093/gji/ggu030 (Online First).

Keylis-Borok VI (1959) On the estimation of the displacement in an earthquake source and of source dimensions. *Annals of Geophysics* 12: 205–214.

Kikuchi M and Kanamori H (1982) Inversion of complex body waves. *Bulletin of the Seismological Society of America* 72: 491–506.

Kikuchi M and Kanamori H (1991) Inversion of complex body waves III. *Bulletin of the Seismological Society of America* 81: 2335–2350.

Knopoff L and Randall MJ (1970) The compensated linear-vector dipole: A possible mechanism for deep earthquakes. *Journal of Geophysical Research* 75: 4957–4963.

Kostrov B (1964) Self-similar problems of propagation of shear cracks. *Journal of Applied Mathematics and Mechanics* 28: 1077–1087.

Kostrov BV (1966) Unsteady propagation of longitudinal shear cracks. *Journal of Applied Mathematics and Mechanics* 30: 1241–1248.

Kostrov B and Das S (1988) *Principles of Earthquake Source Mechanics*. Cambridge: Cambridge University Press.

Kostrov BV and Nikitin L (1970) Some general problems of the mechanics of brittle fracture. *Archiwum Mechaniki Stosowanej* 22: 749–776.

Madariaga R (1976) Dynamics of an expanding circular fault. *Bulletin of the Seismological Society of America* 66: 639–667.

Madariaga R (1978) The dynamic field of Kaskell's rectangular dislocation fault model. *Bulletin of the Seismological Society of America* 68: 869–887.

Madariaga R, Olsen KB, and Archuleta RJ (1998) Modeling dynamic rupture in a 3D earthquake fault model. *Bulletin of the Seismological Society of America* 88: 1182–1197.

Maruyama T (1963) On the force equivalents of dynamical elastic dislocations with reference to the earthquake mechanism. *Bulletin of the Earthquake Research Institute* 41: 467–486.

Nakano H (1923) Notes on the nature of the forces which give rise to the earthquake motions. *Seismological bulletin of the Central Meteorological Observatory of Japan* 1: 92–120.

Rice JR (1980) The mechanics of earthquake rupture. In: Dziewonski AM and Boschi E (eds.) *Physics of the Earth's interior(Proceedings of the International School of Physics 'Enrico Fermi', Course 78, 1979)*, pp. 555–569. Amsterdam: North Holland Publication.

Richards PG (1976) Dynamic motions near an earthquake fault: A three dimensional solution. *Bulletin of the Seismological Society of America* 66: 1–32.

Rosakis AJ, Samudrala O, and Coker D (1999) Cracks faster than the shear wave speed. *Science* 284: 1337–1340.

Sato H and Hirasawa T (1973) Body wave spectra from propagating shear cracks. *Journal of Physics of the Earth* 84: 829–841.

Savage JC (1966) Radiation from a realistic model of faulting. *Bulletin of the Seismological Society of America* 56: 577–592.

Spudich P and Frazer LN (1984) Use of ray theory to calculate high-frequency radiation from earthquake sources having spatially variable rupture velocity and stress drop. *Bulletin of the Seismological Society of America* 74: 2061–2082.

Virieux J (1986) P-SV wave propagation in heterogeneous media: Velocity-stress finite-difference method. *Geophysics* 51: 889–901.

Wald D and Heaton T (1994) Spatial and temporal distribution of slip for the 1992 Landers, California earthquake. *Bulletin of the Seismological Society of America* 84: 668–691.